A structural epidemiological model for the optimal allocation of vaccines across countries

Master Thesis Presented to the

Department of Economics at the

Rheinische Friedrich-Wilhelms-Universität Bonn

In Partial Fulfillment of the Requirements for the Degree of

Master of Science (M.Sc.)

Supervisor: JProf. Dr. Lena Janys

Submitted in July 2021 by:

Manuel Huth

Matriculation Number: 3299004

Contents

List of Figures

List of Tables

1 Introduction

The first case of the COVID-19 pandemic was registered in December 2019 in Wuhan, China (Hui et al., 2020). Up to July 2021, the pandemic has globally caused around 187 million reported infections following around 4 million deaths (ECDC, 2021a). Actual infection counts are estimated to be even higher due to asymptomatic unregistered cases (Byamba-suren et al., 2020). Policymakers have responded to the outbreak of the pandemic with non-pharmaceutical interventions, such as minimizing the contact numbers of individuals in order to reduce the spread of the virus (Gabler et al., 2021). Economists have tried to quantify the costs of these containment measures. Miles et al. (2020) have estimated the costs of the lockdown in the United Kingdom from March 2020 to beginning of June 2020 to be between 100 and 200 billion pounds, which is 5-10% of the United Kingdom's GDP. Deb et al. (2020) have used world-wide data and estimated a 15% loss in industrial production up to 30 days after the implementation of containment measures.

Since the outbreak, more infectious virus mutants have spread, further increasing the physical and social costs. The European Centre for Disease Prevention and Control (ECDC) classifies the virus types into three categories. For (1) *variants of concern*, there is already clear evidence of a significant impact on infections or severity of the disease. For (2) *variants of interest*, this evidence is still preliminary, and (3) *variants under monitoring* have been detected to potentially have the aforementioned impacts (ECDC, 2021c).

Despite the fact that non-pharmaceutical measures and tests have yielded desired reductions in infections (Gabler et al., 2021), the high physical and economical costs have raised the need for vaccinations that provide immunity. In September 2020, more than 100 vaccines against COVID-19 were in the development phase (Mullard, 2020). In late 2020, the first vaccines have been approved. As of July 2021, four vaccines are approved within the European Union (EU) and two are in the development phase (European Commission, 2021b). In mid July 2021, around 65% of adults within the European Economic Area have at least received one shot and about half of the adult population have received full vaccination (ECDC, 2021a). With the agreement of all member states, the European Commission have taken on negotiations with the vaccine suppliers representing the member states. Countries indicate

during the negotiation phase with a manufacturer if they are interested in the respective vaccine. Vaccine doses are subsequently allocated between the interested member states according to their relative population size (European Commission, 2021a).

Our research addresses the question whether the European Union could allocate the purchased vaccines more efficiently through more flexible vaccination strategies than constant rates. Attempting to answer this question, we develop a deterministic Susceptible, Infectious, Recovered, Deceased (SIRD) model with two countries, two vaccines, and two virus types and calibrate it using parameters from the literature. We utilize the real-world vaccine purchase numbers of the EU as exogenous vaccine inflow and scale it down to the population size of our two-country model. Vaccines in our model have varying efficacies with respect to the variants. Variants are distributed heterogeneously across countries. We use piecewise constant functions and logistically transformed cubic Hermite splines as vaccination channels that determine the fractions of the vaccine doses each country receives. Both channels allow the fraction to be non-constant over the time course of the pandemic yielding potentially more complex vaccination strategies. We minimize the number of deaths by optimizing over the parameters of the channel functions, once with additional Pareto constraints and once without the additional constraints. Subsequently, we benchmark the results against the current population size based strategy. We further validate our deterministically derived optimal strategies within a stochastic model.

Closest to our research is the work of Bertsimas et al. (2020). They use a one-country DELPHI model, an extension to the SEIR model, with different regions of the United States to quantify the effects of vaccinations and demographics within one country. Matrajt et al. (2021) examine the optimal vaccination strategy with respect to the prioritization of groups within one country. Tuite et al. (2021) aim to find an optimal policy that allocates vaccines efficiently among first and second vaccine shots.

Our work extends existing research by exploring whether knowledge about the spread of virus types and the respective vaccine efficacies against different types can be used to minimize the number of deceased individuals. We place focus on the importance of policy-wise implementable strategies, such as Pareto improvements with respect to previously applied

2

strategies.

We structure the paper as follows. In Section 2, we introduce our deterministic and stochastic SIRD models, review how the system of differential equations can be derived from modeling the transitions as chemical reactions, and specify the corresponding reactions. In Section 3, we introduce the two vaccination channels and specify the optimization problem for the deterministic model. Section 4 elaborates on the calibration of our model and presents the results. Section 5 concludes.

2   Model

We subdivide the classic SIRD compartments Susceptible (S), Infectious (I), Recovered (R) and Deceased (D), into sub-compartments allowing for heterogeneous areas of residence and vaccination states as well as infections with different virus types. Figure 1 illustrates the general model. Individuals either live in country A or country B. They are non-vaccinated U_0, vaccinated with vaccine one U_1 or vaccinated with vaccine two U_2. Vaccine U_1 represents the messenger ribonucleic acid (mRNA) vaccines and vaccine U_2 represents the vector vaccines. We assume that one vaccination shot is sufficient to get the full protection of vaccine U_1 or U_2. Further, we introduce two virus types. A wild type V_W that serves as baseline variant and a more infectious mutant variant V_M.

To describe our model, we denote every sub-group of individuals by a set $\mathcal{C}_t(F_i)$, where F_i is a placeholder for features that the individuals (elements) within the set $\mathcal{C}_t$ share and t denotes the time at which the set is evaluated. We illustrate the features F_i in the following by providing examples. Let X_h for $h \in \{S, I, R, D\}$ indicate to which general compartment an individual belongs, then, $\mathcal{C}_t(X_S)$ is the set of all susceptible individuals and $\mathcal{C}_t(X_I)$ is the set of all infectious individuals at t. If we want to distinguish not only between general compartments but additionally between countries of residence, we use the feature C_j for $j \in \{A, B\}$ to indicate that the country of residence is j. $\mathcal{C}_t(X_S, C_A)$ is the set of all susceptible individuals of country A and $\mathcal{C}_t(X_S, C_B)$ of country B. Analogously, $\mathcal{C}_t(V_k)$ is the set of all individuals infected with virus k and $\mathcal{C}_t(U_l)$ is the set of all individuals with vaccination
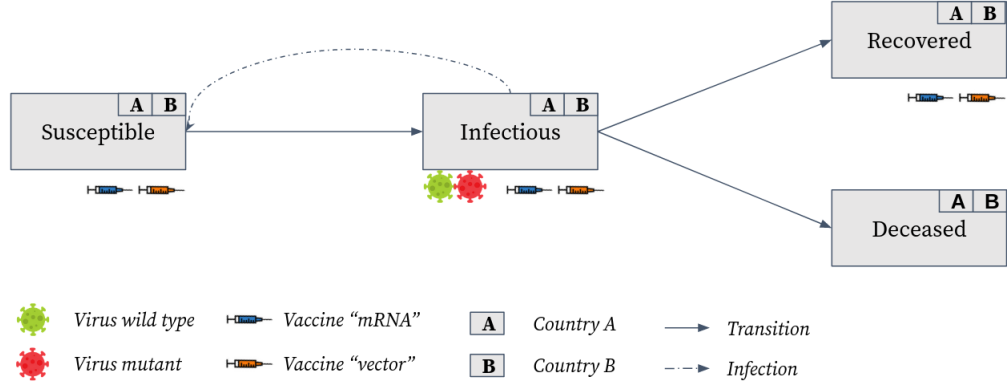
3

Note: Solid lines indicate transition paths and dashed lines indicate infections. Shots below a compartment indicate that individuals from this compartment are vaccinated. Viruses below a compartment indicate that this compartment is infectious. Each compartment is subdivided according to country of residence and vaccination status.

Figure 1: Model structure

status l.

We can link sets with the common set operators, e.g. $\mathcal{C}_t(X_S, C_A) \cup \mathcal{C}_t(X_S, C_B) = \mathcal{C}_t(X_S)$ or $\mathcal{C}_t(X_S) \cap \mathcal{C}_t(X_I) = \emptyset$. The negation operator $\neg$ is used to indicate that a certain feature applies for all but the specified compartment, e.g. $\mathcal{C}_t(\neg X_D)$ is the set of all alive individuals. The cardinality $|\cdot|$ represents the respective number of individuals in a set, e.g. $|\mathcal{C}_t(X_S)|$ equals the number of all susceptible individuals. To shorthand notation, we define $y_t(F_i) = |\mathcal{C}_t(F_i)|$ as the number of individuals within the set $\mathcal{C}_t(F_i)$. By definition, $\mathcal{C}_t() = \cup_{h\in\{S,I,R,D\}}\mathcal{C}_t(X_h)$ is the set of all individuals. Table 1 gives an overview of all features.

We impose a set of assumptions to the compartments in order to rule out undesired cases within the model.

Assumption 1. *For all $t, r \in \mathbb{R}_+$, $k \in \{W, M\}$ and $w \in [-t, \infty)$ let*

$$\mathcal{C}_t(X_I, V_k) \cap \mathcal{C}_{t+r}(X_S) = \emptyset \tag{1.1}$$

$$\mathcal{C}_t(U_1) \cap \mathcal{C}_{t+w}(U_2) = \emptyset \tag{1.2}$$

$$\mathcal{C}_t(C_A) \cap \mathcal{C}_{t+w}(C_B) = \emptyset \tag{1.3}$$

$$\mathcal{C}_t(X_S, V_k) = \emptyset \tag{1.4}$$

Assumption 1.1 rules out reinfections such that an individual that has been infected once

4

Table 1: Notation

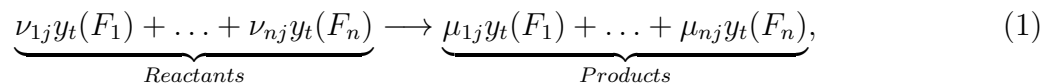| Feature	Code	Indices	Explanation
General compartment	X_h	$h \in \{S, I, R, D\}$	Individuals can either be Susceptible (S), Infectious (I), Recovered (R) or Deceased (D).
Country of residence	C_j	$j \in \{A, B\}$	Individuals can either live in country A or country B.
Virus Type	V_k	$k \in \{W, M\}$	An infection can either be caused by the wild type (W) or the mutant (M) virus. This feature has to be understood, depending on X_h, as *is* or *has been* infected with type k. For example an individual of $\mathcal{C}_t(X_I, V_k)$ *is* currently infected and an individual of $\mathcal{C}_t(X_R, V_k)$ *has been* infected.
Vaccine Type	U_l	$l \in \{0, 1, 2\}$	An individual can either be vaccinated with vaccine 1 or 2 or being unvaccinated (U_0).
Placeholder	F_i	$i \in \mathbb{N}$	A placeholder that is used to address an arbitrary combination of features. $\mathcal{C}_t(F_i)$ should be read as the set of a fixed but arbitrary compartment. If we need to distinguish between two arbitrary compartments, we use F_1 and F_2.

cannot become reinfected after it had recovered. According to Roy (2020), there is evidence that recovered individuals cannot become reinfected but reinfections cannot be ruled out fully. However, the number of reinfected individuals might be negligible, therefore, we do not incorporate reinfections to keep our model parsimonious. Assumption 1.2 implies that an individual only receives one type of vaccine. Receiving one vaccination shot in our model implies that an individual is fully protected according to the vaccine properties, which eliminates the need for a second shot for the same individual. Assumption 1.3 rules out permanent cross-country movements of individuals. We do so since permanent movements should not be a main driver of the pandemic but would require to incorporate more compartments. We refrain from incorporating permanent cross-country movements to keep our model parsimonious. We include cross-border infections by classifying a fraction of infections as cross-border infections. Assumption 1.4 ensures that susceptible individuals cannot be associated with any type of virus. We do so since they have not been infected yet and therefore cannot be classified to one of the two viruses.

2.1 Deterministic model

We use a compartment SIRD model to simulate the pandemic, which is based on a system of ordinary differential equations (ODEs). We see every subcompartment as its own chemical

species and each transition, e.g. vaccinations, infections, recoveries, and deaths, as a chemical reaction. Thus, our system becomes a chemical reaction network. To make this thesis self-contained, we explain how the dynamics of a chemical reaction network are modeled using ODEs. We can limit ourselves to the case of irreversible reactions since recovered and deceased individuals cannot become infectious again, and infectious individuals recover but cannot become susceptible.

Let $\mathcal{C}_t(F_1), \ldots, \mathcal{C}_t(F_n)$ be n pairwise disjoint sets such that their union comprises all individuals $\cup_{i=1}^n \mathcal{C}_t(F_i) = \mathcal{C}_t()$. Every irreversible reaction R_j for $j = 1, \ldots, m$, can be expressed as reaction of all compartments

$$\underbrace{\nu_{1j} y_t(F_1) + \ldots + \nu_{nj} y_t(F_n)}_{Reactants} \longrightarrow \underbrace{\mu_{1j} y_t(F_1) + \ldots + \mu_{nj} y_t(F_n)}_{Products}, \tag{1}$$

where $\nu_{ij} \in \mathbb{N}_0$ and $\mu_{ij} \in \mathbb{N}_0$ are called stoichiometric coefficients. If a compartment $\mathcal{C}_t(F_i)$ is not a reactant or product within reaction R_j, the respective stoichiometric coefficients ν_{ij}, μ_{ij} are set to zero. ν_{ij} describes how much of species $\mathcal{C}_t(F_i)$ is consumed and μ_{ij} how much is produced within reaction R_j. The difference $\mu_{ij} - \nu_{ij}$ is the total change of $y_t(F_i)$ due to one reaction R_j.

We are not only interested in how one reaction (e.g. one infection, one vaccination, etc.) influences the state of the system but rather how often this happens within an interval $[t, t+\tau]$ for $\tau \in \mathbb{R}_+$. If we restrict us to the case $\tau = 1$, the latter is described according to the law of mass action by

$$v_{t,j} = r_j \prod_{i=1}^n y_t(F_i)^{\mu_{ij}}, \tag{2}$$

where r_j is a reaction-specific constant. The product is the number of permutations of individuals that can be part of the reaction. It adjusts the frequency of the reactions by the number of individuals of the respective compartments, e.g. more infectious individuals lead to more subsequent infections.

The change in magnitude of $y_t(F_i)$ within the interval $[t, t+\tau]$ is given by the sum of the

influences of all m reactions

$$y_{t+\tau}(F_i) - y_t(F_i) = \sum_{j=1}^{m} (\mu_{ij} - \nu_{ij}) v_{t,j} \tau. \tag{3}$$

As outlined above, $(\mu_{ij} - \nu_{ij})$ is the stoichiometry that specifies how one reaction influences the system, and $v_{t,j}\tau$ is the number of times reaction R_j happens within the interval $[t, t+\tau]$. Therefore, the product is the influence of R_j on $y_t(F_i)$ within $[t, t+\tau]$. Summed over all reactions, this yields the change of $y_t(F_i)$.

We divide both sides of Equation (3) by τ, let $\tau \to 0$ and plug in Equation (2) to obtain the ordinary differential equation

$$\dot{y}_t(F_i) = \sum_{j=1}^{m} \left[(\mu_{ij} - \nu_{ij}) \, r_j \underbrace{\prod_{k=1}^{n} y_t(F_k)^{\mu_{kj}}}_{v_{t,j}} \right]. \tag{4}$$

We write down the equations for all compartments in matrix form to obtain the system of ODEs, which we use subsequently to ease notation

$$\underbrace{\begin{pmatrix} \dot{y}_t(F_1) \\ \vdots \\ \dot{y}_t(F_n) \end{pmatrix}}_{\dot{Y}(t)} = \underbrace{\begin{pmatrix} \mu_{11} - \nu_{11} & \cdots & \mu_{1m} - \nu_{1m} \\ \vdots & \vdots & \vdots \\ \mu_{n1} - \nu_{n1} & \cdots & \mu_{nm} - \nu_{nm} \end{pmatrix}}_{\mathbf{S}} \cdot \underbrace{\begin{pmatrix} v_{t,1} \\ \vdots \\ v_{t,m} \end{pmatrix}}_{v_t}. \tag{5}$$

If we additionally fix the initial condition $Y(0) = Y_0$, the problem becomes an initial value problem. We use AMICI (Fröhlich et al., 2021) to solve the initial value problem via simulations. AMICI provides the Python interface to interact with the SUNDIALS (Hindmarsh et al., 2005) solvers. We choose the Backward Differentiation Formulas (BDF) methods implemented in SUNDIALS for our implementation of the initial value problem. The BDF, as all numerical solvers we are aware of, discretizes the ODE system to simulate it. Let $\tau_t \in \mathbb{R}_+$ be a varying step size and $q \in \mathbb{N}$ be the order of the BDF. For coefficients $a_k \in \mathbb{R}$ and $b \in \mathbb{R}_+$,

the BDF-q is

$$Y(t) = \sum_{k=1}^{q} a_{t,k} Y\left(t - \sum_{i=1}^{k} \tau_{t-i}\right) + \tau_t b_t \underbrace{\dot{Y}(t)}_{\mathbf{S}v_t}. \tag{6}$$

The function value $Y(t)$ is a linear combination of the last q simulated function values and its derivative. In Equation (3), the baseline function value to determine the next value is the previous function value. In Equation (6), the baseline function value is the weighted sum of the previous q function values. To account for this, the increase of the tangent $\tau_t \dot{Y}(t)$ is corrected by a factor b_t that accounts for the incorporation of the q last function values.

Since v_t depends on Y_t through Equation (2), Equation (6) defines $Y(t)$ implicitly. Thus, it cannot be simulated directly from Equation (6) and numerical methods must be applied. SUNDIALS offers several nonlinear solver choices, such as Newton iteration, to solve this numerical problem. For more details on the implementation of the BDF and the nonlinear solvers see Hindmarsh et al. (2021).

2.2 Stochastic model

We use the stochastic equivalent of our model to test how the derived strategies perform under uncertainty. Gillespie (1977) proposed an algorithm modeling the duration between reactions as random variables that are dependent on the system's state. After one reaction fired, the state is updated and the time to the next period is drawn from the random variable with updated probability distribution. Hence, every probability distribution is based on the latest state of the system and the algorithm is therefore classified as *exact*. On the contrary, approximate algorithms, like $\tau - leaping$ (Gillespie, 2001), group reactions together and use the number of times a reaction happens within an interval as a random variable. However, the reactions within one interval almost surely do not happen at the exact same time. Therefore, the true probability distributions of the second and subsequent reactions, within the interval, must change with respect to the outcome of the previous reactions. By simulating all reactions at once, approximate algorithms do not account for this update of the probability distributions. The drawback of approximation can be justified by a speed-up of approximation methods that are due to fewer function evaluations. Since our model includes a large number of reactions, we decided to use the approximate method and subsequently

dive into the math of it (Gillespie, 2001).

We impose an arbitrary order on all subcompartments. We do so by expressing all compartments by n features $F_1, \ldots F_n$ such that $\cup_{i=1}^n \mathcal{C}_t(F_i) = \mathcal{C}_t()$ and $\mathcal{C}_t(F_1), \ldots, \mathcal{C}_t(F_n)$ are mutually disjoint. We specify the state of the system in terms of the compartments $Y(t) = \begin{pmatrix} y_t(F_1) & y_t(F_2) & \ldots & y_t(F_n) \end{pmatrix}'$. Recall that $\mathbf{S} \in \mathbb{R}^{n \times m}$ is the stoichiometric matrix, as defined in Equation (5), with coefficients s_{ij} and columns $s_{\cdot j}$. R_j for $j = 1, \ldots, m$, is the j-th reaction. Let $K_{t,j}$ be the random variable counting the number of times R_j will fire within the interval $[t, t+\tau)$ for $\tau \in \mathbb{R}_+$. We denote by K_t the random vector collecting the random variables $K_{t,1}, \ldots, K_{t,m}$. Dividing the whole period of interest $[0, T]$ in intervals of length τ, the algorithm is an iterative update of the discretized system's state

$$Y(t + \tau) = Y(t) + \mathbf{S}K_t. \tag{7}$$

Equation (7) is the equivalent of Equation (3), with the only difference that the number of reactions within a given interval are random in Equation (7). Making use of the latter equation, the change in the system's state $\Delta Y(t) = Y(t+\tau) - Y(t) = \mathbf{S}K_t$ can be expressed in terms of a linear combination of the columns of $\mathbf{S}$ with random scalars $K_{t,j}$

$$\Delta Y(t) = \sum_{j=1}^m K_{t,j} \cdot s_{\cdot j}. \tag{8}$$

$s_{\cdot j}$ consists of the stoichiometry for each compartment $\mathcal{C}_t(F_i)$ according to reaction R_j and therefore indicates how the state of the system changes if reaction R_j happens. $K_{t,j}$ is the number of occurrences of reaction R_j. Thus, the product is the system's change due to R_j. Aggregating over all reactions R_j, this yields the total change of the system, similar to the deterministic Equation (3).

So far, we have not specified the distribution of K_t. We are interested in the conditional joint probability distribution $\mathbb{P}_t(K_{t,1} = k_{t,1}, \ldots, K_{t,m} = k_{t,m}|\tau)$ of the random vector $K_t = \begin{pmatrix} K_{t,1}, \ldots, K_{t,m} \end{pmatrix}'$ conditioned on the state of the system and a fixed interval size τ. We define $\mathbb{P}_t$ to be the conditional probability with respect to the state of the system and, therefore, we omit to write the condition explicitly within the condition statement. We

assume independence of all $K_{t,1}, \ldots, K_{t,m}$ such that the problem simplifies to determine the marginal distributions. Let $a_j(y) = \mathbb{P}_t(K_{t,j} = 1 | \tau = 1)$ be the propensity function of the j-th reaction with respect to the state of the system $Y(t) = y$. We assume that for infinitesimal small dt

$$\mathbb{P}_t(K_{t,j} = 1 | \tau = dt) = a_j(y) \cdot dt \tag{9}$$

is the probability that R_j fires once within the interval $[t, t + dt)$ and $(K_{t,j} | Y(t), \tau = dt)$ is Bernoulli $\text{Ber}(a_j(y) \cdot dt)$ distributed. The Bernoulli assumption is justified by choosing dt infinitesimally small, such that R_j fires at most once almost surely.

For simplicity, we assume that $\frac{\tau}{dt}$ is an integer. If we assume that $a_j(y)$ is constant within $[t, t + \tau)$, we can partition the interval in $\frac{\tau}{dt}$ subintervals with length dt. In each of these subintervals the conditional random variable is Bernoulli distributed $(K_{t+s \cdot dt, j} | Y(t), \tau = dt) \sim \text{Ber}(a_j(y) \cdot dt)$ for $s = 0, 1, \ldots, \frac{\tau}{dt} - 1$. Thus, the sum

$$\sum_{s=0}^{\frac{\tau}{dt}-1} (K_{t+s \cdot dt, j} | Y(t), \tau = dt) \sim \text{B}\left(\frac{\tau}{dt}, a_j(y) \cdot dt\right) \tag{10}$$

follows a binomial distribution. The practical problem of this Binomial distribution is that sampling from it requires to define a value for dt. By definition, dt is infinitesimally small and we aim for $dt \to 0$. Fortunately, $dt \to 0$ leads to a Poisson random variable that can be specified by the known τ and $a_j(y)$ such that we can sample from it.

Theorem 1. $B\left(\frac{\tau}{dt}, a_j(y) \cdot dt\right) \xrightarrow{d} Po(a_j(y) \cdot \tau)$ *if* $dt \to 0$.

Proof. The proof is moved to Appendix A.3.3 $\qquad \square$

Armed with the probability distribution of the reactions and an update rule for the states in Equation (7), we can write down the algorithm explicitly.

Algorithm 1: τ-leaping

Result: $Y(t) \quad \forall t \in [0, T]$

Initialize $Y(0) = Y_0, t = 0$, and set fixed $\tau, \mathbf{S}$;

while $t < T$ **do**

    Set y = Y(t);

    Update $a_j = a_j(y)$ for all $j = 1, \ldots, m$;

    Draw $K_{t,j} \sim \text{Po}(a_j \tau)$ for all $j = 1, \ldots, m$;

    Compute $Y(t + \tau) = Y(t) + \mathbf{S}K_t$;

    Store $Y(t + \tau)$;

   Update $t = t + \tau$;

end

2.3 Reactions

From a chemical reaction network's point of view, our model can be divided into three major groups of reactions: 1. Infections, 2. Recoveries and Deaths, and 3. Vaccinations. We group recoveries and deaths since their reactions have the same structure. Subsequently, we state the general and explicit reactions. We define the reactants, products, stoichiometric coefficients, and reaction constants such that the ODE system (5) is determined. Further, we emphasize the reaction constants since they incorporate most of the parameterization into our model.

2.3.1 Infections

Figure 2 depicts the structure of the transitions from the susceptible to the infectious compartments. Every infectious individual $i_1 \in \mathcal{C}_t(x_I)$ can infect a susceptible individual $i_2 \in \mathcal{C}_t(x_S)$ regardless of their countries of residence. However, we account for the higher chance of becoming infected by an individual from the same country by reducing the influence of the infectious compartments from another country via the reaction constants.

In chemical terms, one infectious and one susceptible compartment serve as reactants and
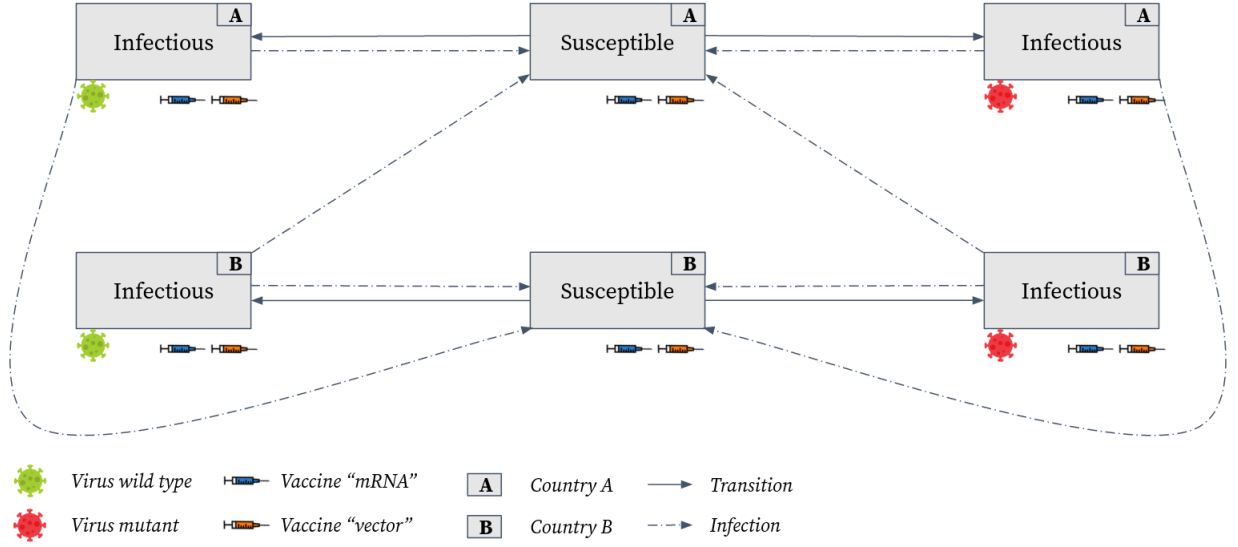
11

Note: Solid lines indicate transition paths and dashed lines indicate infections. Shots below a compartment indicate that individuals from this compartment can be vaccinated. Viruses below a compartment indicate that this compartment is infectious with the respective virus type. The letters in the top right corner of each compartment indicate the country of residence of individuals within the compartment.

Figure 2: Infection structure

yield two infectious compartments that might be subdivided by further features as products

$$y_t(x_I, F_1) + y_t(x_S, F_2) \longrightarrow y_t(X_I, F_1) + y_t(X_I, F_2). \tag{11}$$

We use F_1, F_2 to indicate that the reactions differ with respect to not explicitly mentioned features, e.g. vaccinated individuals have a lower risk of becoming infected or transitioning the virus, the mutant virus is more infectious, and cross-border infections are scaled by a factor to make them comparatively rare events. If $F_1 \neq F_2$, the stoichiometric coefficients are one. If $F_1 = F_2$, they are one for the reactants but two for the product, which is in this case only one compartment. We incorporate the additional features, represented by F_1 and F_2, into the reaction constants, which we label as *infection constants* and define as

infection constant = infections per day × vaccine modifier × compartment adjustment.

In the following, we elaborate how to define the components of the *infections per day*, the *vaccine modifiers*, and the *compartment adjustments*.

To compute the infections per day, we use the average number of contacts between infectious and susceptible individuals and multiply it with the proportion of individuals that become infected while encountering an infectious individual.

Let $c \in R_+$ be the average number of contacts per individual and day and $\alpha \in [0, 1]$ be the proportion of susceptible individuals that become infected when encountering a wild type infected individual without both individuals being vaccinated. Let $\eta \in (1, 1/\alpha]$ be the factor with which the mutant is more infectious than the wild type. Then $\beta = \alpha c$ is the average number of individuals infected per day by i_1 if $i_1 \in \mathcal{C}_t(X_I, V_w, U_0)$. If $i_1 \in \mathcal{C}_t(X_I, V_M, U_0)$, the average infected number increases to $\eta\beta$. We label β as *baseline infection constant* since it covers the most basic case where the reaction happens between an unvaccinated susceptible individual and an unvaccinated wild type infected individual.

Vaccinations influence infections via two channels. First, vaccinated susceptible individuals are less likely to become infected (Callaway, 2021). Second, vaccinated infectious individuals are less likely to transmit the virus (Harris et al., 2021).

To account for the influence of the first channel, we introduce the parameters $\delta_{k,l} \in [0, 1]$, where $k \in \{W, M\}$ indicates the virus type and $l \in \{1, 2\}$ the vaccine type. $\delta_{k,l}$ is the reduction in the probability of becoming infected while encountering an infectious individual after being vaccinated. Thus, susceptible individuals are $1 - \delta_{k,l}$ times less likely to become infected while encountering an infectious individual. This is incorporated within the infection constant by multiplying the baseline infection constant with $1 - \delta_{k,l}$ if $i_s \in \mathcal{C}_t(X_S, U_1) \cup \mathcal{C}_t(X_I, U_2)$.

We account for the second channel by introducing the parameter $\gamma \in [0, 1]$. γ is the reduction in the probability of transmitting the virus after being vaccinated, which we assume to be constant over time and across vaccines. Analogously to the first channel, we multiply the baseline infection constant with $(1 - \gamma)$ if $i_1 \in \mathcal{C}_t(X_I, U_1) \cup \mathcal{C}_t(X_I, U_2)$ to reduce the number of infections caused by a vaccinated individual.

So far, we have only defined the average number of contacts per day c of an infectious individual $i_1 \in \mathcal{C}_t(X_I, F_1)$ but not specified how these contacts are distributed across compartments. We use $\mathbb{P}_t(i_2 \in \mathcal{C}_t(X_S, C_j, F_2)|i_1 \in \mathcal{C}_t(X_I, F_1))$, the conditional probability that

the second individual i_2 is susceptible and from compartment $\mathcal{C}_t(X_S, C_j, F_2)$, and multiply it by β to get the baseline infection constant adjusted by the average number of contacts between i_1 and individuals of the compartment $\mathcal{C}_t(X_S, F_2)$. As introduced in the previous chapter, we omit to condition on $Y(t)$ explicitly within the probability statement $\mathbb{P}_t$ and directly define $\mathbb{P}_t$ to be conditioned on the state of the system $Y(t)$.

We assume that the vaccination status, the type of virus infection, and the exact general compartment (X_S, X_I, X_R) of i_1 are independent of $\mathbb{P}_t(i_2 \in \mathcal{C}_t(X_S, C_j, F_2))$. Thus, the problem facilitates to find $\mathbb{P}_t(i_2 \in \mathcal{C}_t(X_S, F_2)|i_1 \in \mathcal{C}_t(\neg X_D, C_{j'}))$. This independence assumption of the vaccination status implies that for a given number of encounters, an unvaccinated individual i_1 does not change her contact habits compared to her counterfactual vaccinated self. Note that this does not mean that we assume that vaccinated and unvaccinated individuals have the same average number of contacts, since the probabilities are defined conditionally that an encounter occurs, but rather implies that, proportionally, she does not meet more vaccinated individuals than her unvaccinated counterfactual. Differences in the average number of contacts between vaccinated and unvaccinated individuals can be incorporated implicitly via the vaccination parameter $\delta_{k,l}$. To facilitate notation, we subsequently take the perspective that the infectious individual lives in country A. However, the same math applies to country B. We provide a detailed derivation of the probabilities within Appendix A.3.1.

$$\mathbb{P}_t(i_2 \in \mathcal{C}_t(X_S, C_j, F_2)|i_1 \in \mathcal{C}_t(\neg X_D, C_A)) = \begin{cases} 1 - \frac{y_t(X_S, C_j, F_2)}{y_t(\neg X_D)} \cdot b(d(A,B)), & j = A \\ \frac{y_t(X_S, C_j, F_2)}{y_t(\neg X_D)} \cdot b(d(A,B)), & j = B \end{cases} \tag{12}$$

The probability is essentially the relative population size adjusted by a penalty function $b : \mathbb{R}_+ \to [0,1]$ that depends on the distance between both countries $d(A,B)$ and accounts for fewer cross-border encounters. By mapping the distance into the unit interval, we allow the probability of a cross-border encounter to be at most as high as the relative population size. The distance can be interpreted as geographical distance but it could also serve to incorporate other factors, like favored holiday destinations, that encourage or discourage

cross-border encounters. We impose three conditions on the function b

$$\lim_{d \to \infty} b(d) = 0 \tag{B.1}$$

$$b(0) = 1 \tag{B.2}$$

$$b(d_1) < b(d_2) \quad \text{if } d_1 > d_2. \tag{B.3}$$

Condition $(B.1)$ ensures that countries that have a large distance have only small influences on each other. $(B.2)$ defines a rather theoretical case where cross-border encounters are as likely as within-country encounters. $(B.3)$ ensures that countries that have a greater distance have a smaller influence on each other.

With the derived specifications of the infections per day, the vaccine modifiers, and the compartment adjustments, we can specify the compartment-specific infection constants. We illustrate this with two examples.

Example 1. *Let the reactants be the compartments $\mathcal{C}_t(X_I, C_A, V_W, U_0)$ and $\mathcal{C}_t(X_S, C_B, U_0)$. The corresponding reaction is*

$$y_t(X_I, C_A, V_W, U_0) + y_t(X_S, C_B, U_0) \xrightarrow{r_{j_1}} y_t(X_I, C_A, V_W, U_0) + y_t(X_I, C_B, V_W, U_0), \tag{13}$$

where r_{j_1} denotes the infection rate. To account for the infections per day, we use the baseline infection constant β since the infectious compartment is infected with the wild type. The susceptible and the infectious compartments are unvaccinated. Therefore, we do not multiply with a vaccine modifier. The compartments are, however, from different countries. We therefore adjust by multiplying with $\frac{y_t(X_S, C_B, F_2)}{y_t(\neg X_D)} \cdot b(d(A, B))$

$$r_{j_1} = \beta \cdot \frac{y_t(X_S, C_B, F_2)}{y_t(\neg X_D)} \cdot b(d(A, B)) \tag{14}$$

Example 2. *For the second example, we consider vaccinated and mutant infected compartments $\mathcal{C}_t(X_I, C_A, V_M, U_1)$ and $\mathcal{C}_t(X_S, C_B, U_2)$ as reactants to showcase the influence of the*

vaccine and the mutant modifier.

$$y_t(X_I, C_A, V_M, U_1) + y_t(X_S, C_B, U_2) \xrightarrow{r_{j_2}} y_t(X_I, C_A, V_M, U_1) + y_t(X_I, C_B, V_M, U_2). \quad (15)$$

Since the infectious individual is infected with the mutant, we multiply the baseline infection constant with η. Since the infectious compartment is vaccinated, we multiply the constant with $(1 - \gamma)$. Since the susceptible compartment is vaccinated with vaccine U_2, we multiply the infection constant with $1 - \delta_{M,2}$. The compartments are from different countries. We therefore adjust by multiplying with $\frac{y_t(X_S, C_B, F_2)}{y_t(\neg X_D)} \cdot b(d(A, B))$

$$r_{j_2} = (1 - \delta_{M,2})(1 - \gamma)\eta\beta\frac{y_t(X_S, C_B, F_2)}{y_t(\neg X_D)} \cdot b(d(A, B)). \quad (16)$$

To ensure readability, we refrain from writing down all exact infections but they can be derived as shown in the two examples and are depicted in Figure 2.

2.3.2   Recoveries and deaths
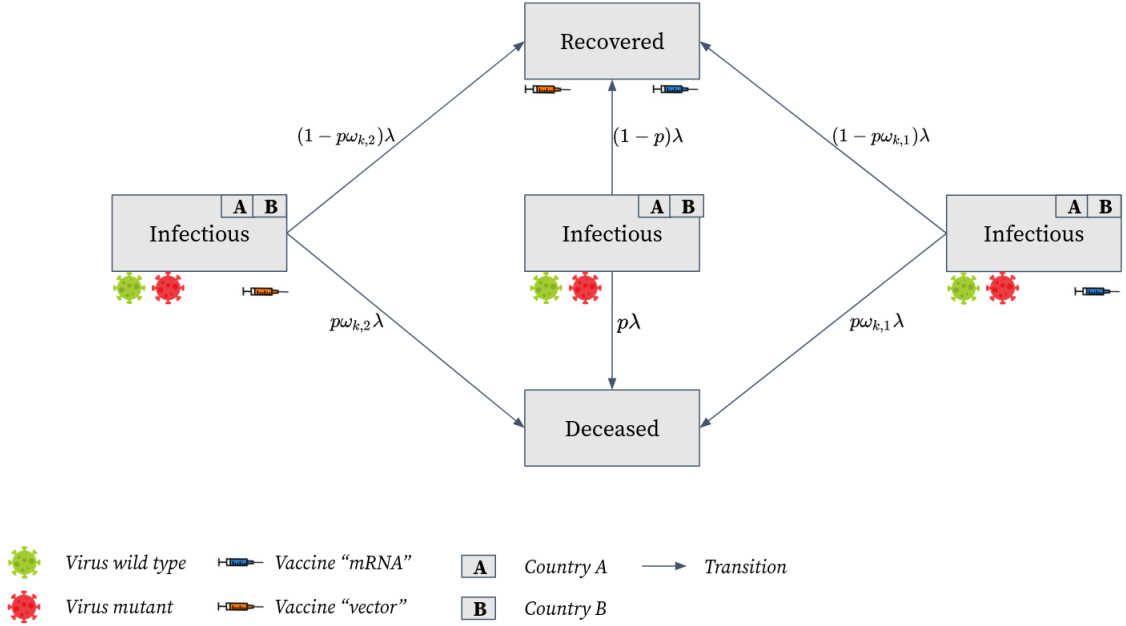
Note: Solid lines indicate transition paths. Shots below a compartment indicate that individuals from this compartment are vaccinated. Viruses below a compartment indicate that this compartment is infectious with the respective virus type. The letters in the top right corner of each compartment indicate the country of residence of individuals within the compartment. The formulas on top of the solid lines indicate the respective reaction constant.
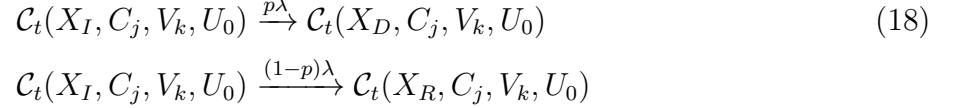
Figure 3: Recovery and death structure

Figure 3 depicts the dynamics of the recoveries and deaths. The general reactions are defined by one infectious reactant and one product

$$\mathcal{C}_t(X_I, F_1) \longrightarrow \mathcal{C}_t(X_D, F_1) \tag{17}$$

$$\mathcal{C}_t(X_I, F_1) \longrightarrow \mathcal{C}_t(X_R, F_1).$$

The change in mass of the reactants (decrease) and the products (increase) is the product of the average number of individuals transitioning out of the infectious compartment $\mathcal{C}_t(X_I, F_1)$ and the fraction of individuals that transition to the product compartment, either $\mathcal{C}_t(X_D, F_1)$ or $\mathcal{C}_t(X_R, F_1)$.

Let $\lambda \in \mathbb{R}_+$ be the average number of individuals that transition out of $\mathcal{C}_t(X_I, F_1)$. We assume that a constant fraction $p \in [0, 1]$ of these individuals dies. Hence, $p\lambda$ individuals transition to the deceased and $(1 - p)\lambda$ individuals transition to the recovered state. The explicit reactions for unvaccinated individuals are for $j \in \{A, B\}$ and $k \in \{W, M\}$

$$\mathcal{C}_t(X_I, C_j, V_k, U_0) \xrightarrow{p\lambda} \mathcal{C}_t(X_D, C_j, V_k, U_0) \tag{18}$$

$$\mathcal{C}_t(X_I, C_j, V_k, U_0) \xrightarrow{(1-p)\lambda} \mathcal{C}_t(X_R, C_j, V_k, U_0)$$

$1/\lambda$ is the average duration an individual spends within $\mathcal{C}_t(X_I, F_1)$. We have implicitly assumed that this time is the same for dying and recovering individuals, which might not be accurate in real-world examples since dying individuals have more severe cases and heavier viral loads, such that they stay infectious longer. However, incorporating separated average durations would raise the need for more compartments. Since we allow for vaccinations of recovered and infectious individuals, slower transitions to the recovered compartments do not bias the vaccine allocation. Therefore, we assume that this simplification is negligible. Moreover, note that p does not depend on the virus type. The virus type therefore only influences the number of infections but not the probability of dying for infected individuals. According to Davies et al. (2021), this assumption might be violated due to higher mortality of mutants. However, we do so since the difference is rather small and we want to keep our model simple.

If the infectious individuals are vaccinated, they are less likely to decease (Tenforde, 2021; Voysey et al., 2021). To account for this reduction in the fraction that transitions to the deceased state, we introduce the parameters $\omega_{k,l} \in [0,1]$ for $k \in \{W, M\}$ and $l \in \{1, 2\}$. We use $p\omega_{k,l}$ as a new probability of dying due to being infected with virus k after being vaccinated with vaccine l. $\omega_{k,l}$ is thus the reduction in the probability of dying. The corresponding reactions for vaccinated individuals are for $j \in \{A, B\}, k \in \{W, M\}$ and $l \in \{1, 2\}$

$$\mathcal{C}_t(X_I, C_j, V_k, U_l) \xrightarrow{p\omega_{k,l}\lambda} \mathcal{C}_t(X_D, C_j, V_k, U_l) \tag{19}$$
$$\mathcal{C}_t(X_I, C_j, V_k, U_l) \xrightarrow{(1-p\omega_{k,l})\lambda} \mathcal{C}_t(X_R, C_j, V_k, U_l).$$
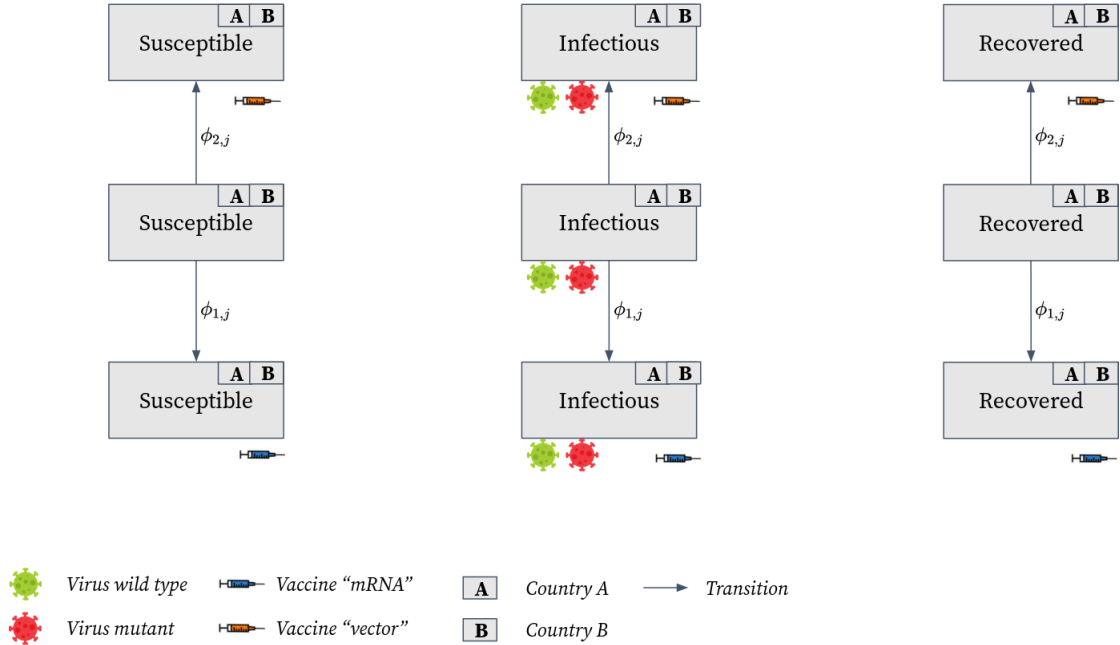
2.3.3 Vaccination

Note: Solid lines indicate transition paths. Shots below a compartment indicate that individuals from this compartment are vaccinated with the respective vaccine. Viruses below a compartment indicate that this compartment is infectious. The letters in the top right corner of each compartment indicate the country of residence of individuals within the compartment. The formulas next to the solid lines indicate the respective reaction constant.

Figure 4: Vaccination structure

Figure 4 depicts the vaccination dynamics. We allow for vaccinations of susceptible, recovered, and deceased individuals. We vaccinate susceptible individuals to protect them from becoming infected. We vaccinate infectious individuals to account for asymptomatic cases (Byambasuren et al., 2020) that receive the vaccine in the real world. Adding asymptomatic

18

infectious compartments would make the model more realistic but increases the number of compartments by 36. We therefore decided to refrain from incorporating it but remark that this could be subject to further research. We vaccinate recovered individuals to consider the vaccine doses taken by them. The latter are vaccinated within the real world to increase their immunity (Skelly et al., 2021). Since we use real-world vaccine inflow, we found it plausible to incorporate vaccinations of recovered individuals into our model.

Let $\phi_{l,j} \in \mathbb{R}_+$ be the vaccination constant of vaccine l in country j at time t. The vaccination constant of a vaccine is assumed to be equal for all vaccination subcompartments of S, I, R within one country, indicating that the decision to vaccinate an individual is independent of whether the individual is susceptible, infectious, or recovered. The corresponding reactions are for $j \in \{A, B\}$, $k \in \{W, M\}$ and $l \in \{1, 2\}$

$$\mathcal{C}_t(X_S, C_j, U_0) \xrightarrow{\phi_{l,j}} \mathcal{C}_t(X_S, C_j, U_l) \tag{20}$$
$$\mathcal{C}_t(X_I, C_j, V_k, U_0) \xrightarrow{\phi_{l,j}} \mathcal{C}_t(X_I, C_j, V_k, U_l)$$
$$\mathcal{C}_t(X_R, C_j, V_k, U_0) \xrightarrow{\phi_{l,j}} \mathcal{C}_t(X_R, C_j, V_k, U_l).$$

The vaccination constant is determined by the implemented vaccination strategy. How the vaccination constant is derived given a vaccination strategy, we explain in Chapter 3.

3 Optimal vaccine allocation

The task of allocating the vaccines across countries raises the need to specify the number of available vaccine shots. We define the number of available vaccines at any time t as exogenous and calibrate it based on the true number of COVID-19 vaccines that have been allocated to the EU within the start of 2021 and mid July 2021.
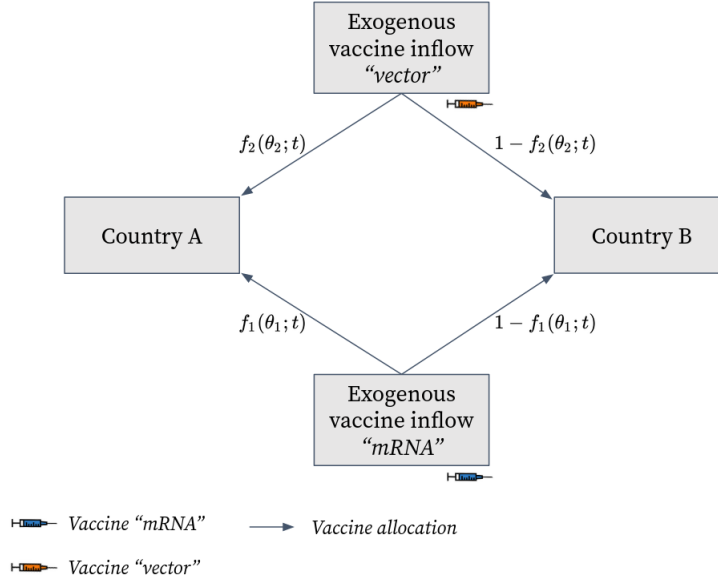
Note: Solid lines indicate vaccine allocations to a country. Shots below a box indicate the type of vaccines. The formulas next to the solid lines indicate the respective fractions of vaccines that are assigned to the country. The fractions depend on a parameter vector θ_l, over which we optimize to find the optimal solution.

Figure 5: Vaccine inflow and allocation across countries

Let $W_{l,j}(t)$ be the number of vaccination shots of vaccine l available at time t in country j and $W_l(t) = W_{l,A}(t) + W_{l,B}(t)$ be the total number of available vaccine shots of vaccine l at t. We assume that all vaccine shots are vaccinated immediately.

Assumption 2. *The total number of vaccine l available in country j equals the number of vaccinated individuals in country j for all $t \in [0, T]$.*

$$\underbrace{W_{l,j}(t)}_{\substack{\text{Total number of} \\ \text{vaccine } l \text{ doses in} \\ \text{country } j \text{ at time } t}} = \underbrace{\phi_{l,j} \cdot y_t(\neg X_D, C_j, U_0)}_{\substack{\text{Number of individuals} \\ \text{vaccinated with } l \\ \text{at time } t}}. \tag{21}$$

Within the real world, vaccinations take around 2 weeks to yield full protection (CDC, 2021). In this regard, our model can be interpreted such that the number of lately vaccinated indi-

viduals is the number of individuals who have recently received full protection by the vaccine. The vaccination constant would then be the constant defining the reaction of becoming protected.

At each point in time t, country A receives a fraction $f_l(\theta_l; t)$ with $f_l : \mathbb{R}^z \times [0, \tau] \to [0, 1]$ of vaccine W_l. The fraction depends on the time t and a parameter vector $\theta_l \in \mathbb{R}^z$ that parameterizes $f_l(\theta_l; t)$.

We assume that all vaccine doses stay within the two countries and none of them are wasted

Assumption 3. *The total number of vaccine shots available in country j at time t is equal to the number of shots assigned to it through the vaccination strategy*

$$W_{l,A}(t) = f_l(\theta_l; t) W_l(t) \tag{22}$$

$$W_{l,B}(t) = [1 - f_l(\theta_l; t)] W_l(t).$$

We use Assumption 2 and Assumption 3 to solve for the vaccination constants. They depend on the vaccine inflow, the fraction of vaccines assigned to the respective country, and the total number of individuals that potentially can be vaccinated within the country

$$\phi_{l,A} = \frac{f_l(\theta_l; t) W_l(t)}{y_t(\neg X_D, C_A, U_0)}$$

$$\phi_{l,B} = \frac{[1 - f_l(\theta_l; t)] W_l(t)}{y_t(\neg X_D, C_B, U_0)}$$

if $y_t(\neg X_D, C_j, U_0) > 0$ for $j \in \{A, B\}$ respectively. Otherwise, $\phi_{l,j} = 0$. Note that the vaccination constant is actually not a constant since it depends on time dependent parameters. This is, however, just a naming convention that has no further implications for our model.

3.1 Objective function

Given a functional form of f_l, a specific $\bar{\theta}_l \in \mathbb{R}^z$ is called a *strategy* for vaccine l. A *vaccination strategy* $\bar{\Theta} = \begin{pmatrix} \bar{\theta}_1 \\ \bar{\theta}_2 \end{pmatrix}$ is a collection of strategies defined for both vaccines. We label the strategy

Θ_{EU} that assigns the relative population size of country A to be the fraction of vaccines assigned to country A,

$$f_l(\theta_{EU}, t) = \frac{y_0(\neg X_D, C_A)}{y_0(\neg X_D)}, \tag{23}$$

as *current EU strategy* or *current strategy* (European Commission, 2021a). Within the real world, member states of the EU can refrain from buying their entire assigned quantity and and thus give other member states the chance to buy it. We account for this implicitly within our optimization, since every allocation can be seen as a case where one country waives its right for a certain amount of vaccine doses, which is therefore taken by the other country.

We denote the number of deceased individuals in country A, conditioned on the current strategy, by $y_T(X_D, C_A; \Theta_{EU})$ and the corresponding number in country B by $y_T(X_D, C_B; \Theta_{EU})$. We use this strategy as a baseline case to examine how we can improve using an optimal strategy. An optimal strategy Θ^* is the solution to the minimization problem

$$\begin{aligned}
\arg\min_{\Theta \in \mathbb{R}^{2z}} \quad & y_T(X_D) \\
\text{subject to} \quad & \phi_{l,A} = \frac{f_l(\theta_l; t) W_l(t)}{y_t(\neg X_D, C_A, U_0)} && \text{for } l \in \{1, 2\}, && \text{(C.1)} \\
& \phi_{l,B} = \frac{[1 - f_l(\theta_l; t)] W_l(t)}{y_t(\neg X_D, C_B, U_0)} && \text{for } l \in \{1, 2\}, && \text{(C.2)} \\
& \Theta = \begin{pmatrix} \theta_1' & \theta_2' \end{pmatrix}', && && \text{(C.3)} \\
& \beta, \eta, \gamma, \delta_{k,l}, \omega_{k,l}, Y(0), W_l(t) && && \text{(C.4)}
\end{aligned}$$

and we call it an *optimal vaccination strategy* for the given minimization problem. Conditions $C.1$, $C.2$, and $C.3$ indicate how the parameter vector Θ affects the model. $C.4$ specifies that all exogenous parameters are set to constant values.

If additionally constraints $C.5$ and $C.6$ are satisfied,

$$y_T(X_D, C_A) < y_T(X_D, C_A; \Theta_{EU}) \tag{C.5}$$

$$y_T(X_D, C_B) < y_T(X_D, C_B; \Theta_{EU}) \tag{C.6}$$

the optimal strategy is Pareto optimal and we call it *Pareto optimal vaccination strategy*. The Pareto optimality constraints ensure that both countries have fewer deceased individuals as with the current strategy. Taking the perspective that both countries can veto against strategies, non-Pareto optimal strategies might not be implementable since no country would agree to deviate from the current strategy if it experiences more deceased individuals with the new strategy.

We follow Bertsimas et al. (2020) and choose the total number of deceased individuals as objective. We decided to do so such that the death protection parameters $\omega_{k,l}$ influence the solution. Other objectives like the total number of infectious individuals, a combination of both, or an objective that takes long-term measures into account could be considered as well are subject to further research.

3.2 Vaccine allocation channels

We examine two functional forms of f_l. First, f_l is a stepwise function. Second, f_l is a logistically transformed third-order spline function. Both forms can be parameterized using the parameter vector θ_l. Both forms do not yield constructive vaccination strategies since we do not link the vaccine allocation directly to the state of the model but rather optimize over time-dependent parameters.

To define the functional forms, we subdivide the interval $[0, T]$ into a tagged partition $0 = t_0 < t_1 < \cdots < t_z = T$. Let $\mathcal{T}_i = [t_{i-1}, t_i)$ for $i = 1, \ldots, z$, be the corresponding intervals of the tagged partition. We label $\mathcal{T}_i$ as the *i-th decision period*. To be more precise on the functional form of f_l, we subdivide the parameter vector into its components $\theta_l = \begin{pmatrix} \theta_{l,1} & \theta_{l,2} & \ldots & \theta_{l,z} \end{pmatrix}'$.

In a world with a piecewise constant vaccination channel, policymakers determine a fraction that is allocated to country A for a fixed decision period $\mathcal{T}_i$, evaluate, and then adjust before the next decision period T_{i+1} begins. In Figure 6 (first plot), we show an exemplary vaccination strategy for vaccine l.

In mathematical terms, every $\theta_{l,i} \in [0,1]$ is assigned to an interval $\mathcal{T}_i$. The parameters $\theta_{l,i}$ are in this case the fractions of vaccines assigned to country A.

$$f_l(\theta_l; t) = \theta_{l,i} \quad \forall t \in \mathcal{T}_i. \tag{25}$$

Note that the current EU strategy is a special case of a step function that has $\theta_{l;1} = \theta_{l,2} = \ldots = \theta_{l,z} = y_0(\neg X_D, C_l)/y_0(\neg X_D)$, assuming that the allocations are not adjusted for changes in the population sizes over the course of the pandemic.
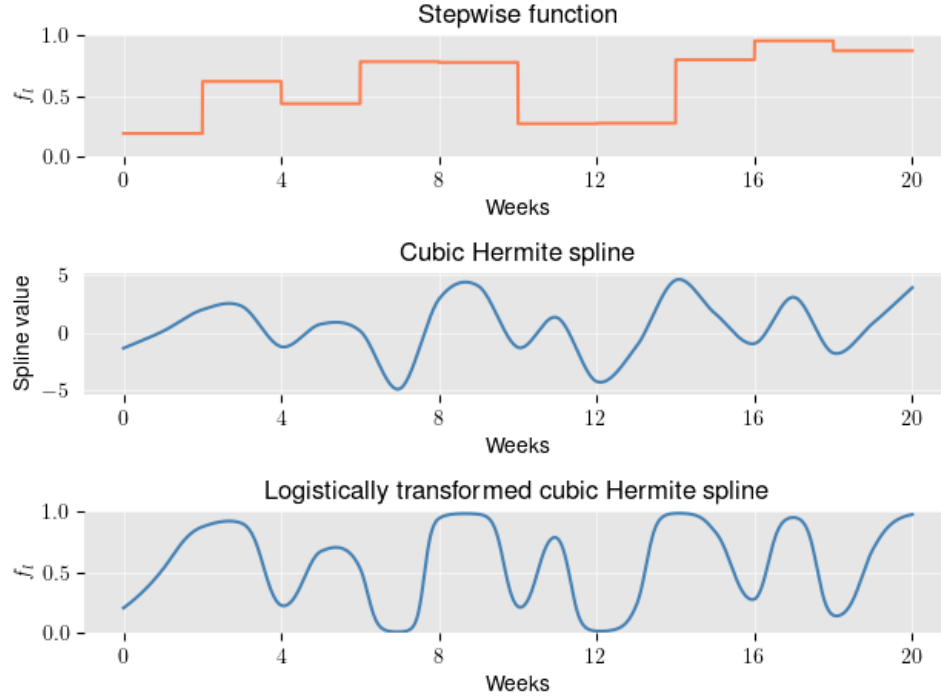
Note: Examples of a piecewise vaccine allocation in orange and a spline allocation in blue. The first graph depicts the values of the spline and the second graph shows the corresponding transformed function that maps the values into the unit interval. The third graph shows a different approach using a piecewise constant function. Decision intervals have a duration of 2 weeks.

Figure 6: Exemplary vaccination strategies with respect to the two vaccination channels

In a world with spline vaccination channels, policymakers decide on the start and end values of the vaccine allocations within each interval $\mathcal{T}_i$. Given the boundary values, one polynomial for each interval $\mathcal{T}_i$ is computed and logistically transformed to meet the unit interval domain of the fractions. Figure 6 shows an exemplary spline (second plot) and how it is shrunk into the unit interval via the logistic function (third plot). By using polynomials rather than constant functions, we allow for more complex policy decisions within one decision

period $\mathcal{T}_i$ since fluctuations within one decision period can be taken into account. However, one should note that this exercise is rather theoretical and aims to show what strategies could be achieved theoretically. We use splines instead of a global polynomial interpolation because they are practical with respect to construction and because global interpolations might suffer from undesired properties, as in Runge's phenomenon (Runge, 1901).

Given a polynomial from the third-order polynomial ring over the real numbers $P_{l,i}(t) \in \mathbb{R}_3(t)$, the fraction is mathematically described by the composition of the polynomial and the logistic function

$$f_l(\theta; t) = \frac{1}{1 + \exp\left(-P_{l,i}(t)\right)} \quad \forall t \in \mathcal{T}_i. \tag{26}$$

We choose $P_{l,i}(t)$ to be in cubic Hermite form. The name cubic arises from the condition that every $P_{l,i}(t)$ is at most a third-order polynomial. The name Hermite indicates that the derivatives at the boundaries $P'_{l,i}(t_{i-1})$ are approximated using finite differences. We use central finite differences for non-boundary values and forward as well as backward finite differences at the respective boundaries t_0 and t_z

$$\begin{aligned} P'_{l,1}(t_0) &\approx \frac{P_{l,1}(t_1) - P_{l,1}(t_0)}{t_1 - t_0} \\ P'_{l,i}(t_{i-1}) &\approx \frac{1}{2}\left[\frac{P_{l,i}(t_i) - P_{l,i}(t_{i-1})}{t_i - t_{i-1}} + \frac{P_{l,i-1}(t_{i-1}) - P_{l,i-1}(t_{i-2})}{t_{i-1} - t_{i-2}}\right] \\ P'_{l,z}(t_z) &\approx \frac{P_{l,z}(t_z) - P_{l,z}(t_{z-1})}{t_z - t_{z-1}}. \end{aligned} \tag{27}$$

Equipped with the two functional values at the boundaries and approximations for their derivatives, we have four conditions to specify the polynomial of order three. Thus, we can parameterize the splines by specifying the polynomial values at the boundaries in terms of θ_l by setting the function values at the boundaries equal to the respective coefficient

$$\begin{aligned} P_{l,i}(t_{i-1}) &= \theta_{l,i-1} \\ P_{l,i}(t_i) &= \theta_{l,i}. \end{aligned} \tag{28}$$

The polynomial $P_{l,i}(t)$ is given as a linear combination of four basis polynomials $B_1(t)$,

$B_2(t)$, $B_3(t)$ and $B_4(t) \in \mathbb{R}_3(t)$ with the boundary values of the polynomial and its derivative. Let $t' = (t - t_{i-1})/(t_i - t_{i-1})$ for $t \in \mathcal{T}_i$ and

$$
\begin{aligned}
P_{l,i}(t) = B_1(t') \overbrace{P_{l,i}(t_{i-1})}^{\theta_{l,i-1}} &+ B_2(t')(t_i - t_{i-1})P'_{l,i}(t_{i-1}) \\
&+ B_3(t') \underbrace{P_{l,i}(t_i)}_{\theta_{l,i}} + B_4(t')(t_i - t_{i-1})P'_{l,i}(t_i) \quad \forall t \in \mathcal{T}_i.
\end{aligned}
\tag{29}
$$

The scalars of the linear combination are dependent on the parameter vector θ_l through (27) and (28). The basis polynomials are defined by $B_1(t) = 2t^3 - 3t^2 + 1$, $B_2(t) = t^3 - 2t^2 + t$, $B_3(t) = -2t^3 + 3t^2$ and $B_4(t) = t^3 - t^2$. Note that the imposed structure of $P_{l,i}(t)$ is well-defined, which can be verified by evaluating the polynomial and its derivative at the boundaries t_{i-1} and t_i. We provide the calculations in Appendix A.3.2.

We show that the basis polynomials indeed form a basis of $\mathbb{R}_3(t)$. Showing the basis property proves that the four polynomials span $\mathbb{R}_3(t)$ and therefore we do not exclude any polynomials from the space of policies that could be implemented.

Theorem 2. $B_1(t) = 2t^3 - 3t^2 + 1$, $B_2(t) = t^3 - 2t^2 + t$, $B_3(t) = -2t^3 + 3t^2$, $B_4(t) = t^3 - t^2 \in \mathbb{R}_3(t)$ *form a polynomial basis of* $\mathbb{R}_3(t)$.

Proof. The proof is moved to Appendix A.3.4. $\qquad\square$

4 Simulation and optimization

We use values derived from the literature to calibrate our models' fixed parameters. We simulate one model using a stepwise vaccination strategy and one model using spline vaccination strategy. Stepwise and spline vaccination channels yielded very similar results regarding the vaccination strategies and the trajectories of the compartments, which we see as enhancement of the robustness of our findings. However, we refrain from showing the same results twice and move the results from the stepwise approach to Appendix A.2.1. Sensitivity checks are moved to Appendix A.1.

4.1 Calibration

Within our model there exist two vaccines U_1 and U_2. Whereas in the EU, as of July 2021, 4 vaccines have been approved and two are in the development phase (European Commission, 2021b). To establish the link from our theoretical model to the real-world COVID-19 vaccines, we use data based on the four approved vaccines to calibrate our model. Vaccine U_1 represents the messenger ribonucleic acid (mRNA) vaccines and vaccine U_2 represent the vector vaccines.

Currently EU-approved mRNA vaccines are Comirnaty, also known as BNT162b2, from Pfizer-BioNTech as well as Spikevax, also known as mRNA-1273, from Moderna. The approved vector vaccines are Vaxzevria from Oxford-Astra Zeneca as well as Janssen, also known as Johnson & Johnson COVID-19 vaccine, from Janssen Vaccines.

We use efficacy values reported within the literature to calibrate the vaccine-specific parameters $\delta_{k,l}$ and $\omega_{k,l}$. Efficacy describes the effect with respect to perfect conditions, whereas effectiveness measures the effect under real-world clinical settings (Gartlehner et al., 2006). Therefore, real-world effectiveness could be lower than the numbers reported in Table 2. We use data from the early Alpha virus type to calibrate the wild type parameters and data from the lately spreading Delta variant to calibrate the mutant parameters. In contrast to conventional vaccines, mRNA vaccines do not contain viral proteins themselves. They only contain the information human cells need to produce a virus trait that triggers the desired immune response (Biontech, 2021). This new method has shown a significant improvement concerning immunity, yielding higher efficiacy values as can be seen in Table 2.

Due to the recent spread of the Delta variant, data is still limited and we did not find reliable sources for the Delta-efficacy of Spikevax and Janssen. For the latter, a recent study by Jongeneelen et al. (2021) reports that even though real-world effectiveness has been shown, they found no efficacy for the Janssen vaccine against the Delta variant. Since their study only included 8 individuals, we refrain from using the study to calibrate our model.

With respect to Table 2, we decided to set the protection of the mRNA vaccines against infection with the wild type (Alpha variant) to be $\delta_{1,W} = 0.94$ and against infection with the

Vaccine	Efficacy		Sources
	Alpha	Delta	
Comirnaty	94%-95%	87%-95%	Callaway (2021), Nasreen et al. (2021), Polack et al. (2020), Prüß (2021), Sheikh et al. (2021)
Spikevax	94%	-	Oliver (2021b), Prüß (2021)
Vaxzevria	66%-73%	60%-71%	Callaway (2021), Emary et al. (2021), Prüß (2021), Stowe et al. (2021)
Janssen	66%	-	Oliver (2021a), Sadoff et al. (2021)

Note: Efficacy is measured as protection against an infection after 14 days of the second vaccine shot.

Table 2: Vaccine efficacy

mutant (Delta variant) to be $\delta_{1,M} = 0.9$. For the vector vaccines, we chose for the wild type $\delta_{2,W} = 0.7$ and for the mutant $\delta_{2,M} = 0.65$.

Abu-Raddad et al. (2021) report Comirnaty to protect from hospitalization by 97.4%. Tenforde (2021) finds that Comirnaty and Spikevax yield 94% protection against hospitalization within the age group of ≥ 65 aged individuals. Voysey et al. (2021) report a 100% efficacy against hospitalization regarding Vaxzevria and the Alpha variant. We generalize the empirical results and set the values of death protection $\omega_{k,l} = 0.99$ for all $k \in \{W, M\}$ and $l \in \{1, 2\}$.

Harris et al. (2021) found in a study of more than 365,000 British households, mixed with vaccinated and unvaccinated individuals, that full vaccination with Comirnaty or Vaxzevria reduces the transmission probability by 40%-60%. We therefore set $\delta = 0.5$. We found within our sensitivity checks that the exact magnitude of γ does not change the results qualitatively, see Appendix A.1.3.

The basic reproduction number R_l of virus type l is the average number of unvaccinated individuals infected by one unvaccinated infectious individual. Translated to our model, this yields the following equations

$$R_W = \frac{\beta}{\lambda}$$

$$R_M = \frac{\eta\beta}{\lambda},$$

(30)

Recall that $1/\lambda$ is the average time an individual is infected and β, or $\eta\beta$, is the average number of individuals infected by one infectious individual per day. The German Robert Koch Institut (2021) reports the basic reproduction number to be between 2.8 and 3.8. Moreover, they state that an individual is infectious for about ten days. We use $\lambda = 0.1, R_W = 3$ and $R_M = 3.6$, yielding $\beta = 0.3$ and $\eta = 1.2$. Note that these numbers do not take non-pharmaceutical measures such as testing and social distancing into account, which would lower the infection constant. Therefore, our simulated pandemic might have higher death numbers and be terminated earlier than the real-world COVID-19 pandemic.

Baud et al. (2020) find a death rate of 5.7% for symptomatic cases. However, this overestimates the true death rate due to undetected asymptomatic cases that did not result in deaths. Wu and McGoogan (2020) account for asymptomatic cases and find estimates to be between 2%-3%. We therefore use $p = 2.5\%$ for our simulations.

To define the initial value problem, we set the initial population size of susceptible individuals in both countries to $y_0(X_S, C_A) = y_0(X_S, C_B) = 80$ million, a country size similar to Germany. Country A starts with ten wild type infectious individuals $y_0(X_I, C_A, V_W) = 10$ and country B with ten mutant type infected individuals $y_0(X_I, C_B, V_M) = 10$. We initially separate the virus types by country to examine the influence of heterogeneous virus infectiousness of upcoming mutants across countries. All other compartments are set to zero at the beginning.

To specify the cross-border encounter modifier $b(d(A, B))$, we use tourism data from Germany and France. We use France since it is population-wise the largest country with a border to Germany. In 2016, $1,725,854$ individuals from France traveled to Germany and stayed for two days on average (Statistisches Bundesamt, 2017). We divide this number by 366 to get an estimate of the average number of French individuals in Germany at each day in 2016 and scale it by $\frac{80}{67}$ to adjust that our second country has a population size of 80 million, whereas France has around 67 million inhabitants $\frac{2 \cdot 1,725,854}{366} \cdot \frac{80}{67} \approx 11,261$. Assuming that the same number of French individuals have been in Germany every day and using equation (34) with a constant proportion $y_t(\neg X_D, C_B)/y_t(\neg X_D) \approx y_0(\neg X_D, C_B)/y_0(\neg X_D) \quad \forall t \in [0, T]$,

this yields

$$b(d(A, B)) = \frac{11,261}{80,000,000} \approx 0.0002$$

Note that this estimate is rather conservative since we do not take commuters and unregistered visits, such as shopping trips, into account. You find a section about the sensitivity of the model with respect to $b(d(A, B))$ within Appendix A.1.1.

We set the length of the whole decision period to $T = 140$ and subdivide the length of each decision interval $\mathcal{T}_i$ to 14 days. Even though we derive the model's parameters using days, we subsequently use weeks to label the axes to increase readability of the figures.

Figure 7 depicts the inflow of both vaccines. The daily vaccine inflow $W_l(t)$ is computed using EU data of the vaccine inflow taken from the open-source data bank of the ECDC (2021b). The data reports the weekly inflow of vaccines for all countries within the EU. We accumulate the numbers of Corminarty and Spikevax to compute the total numbers of mRNA vaccines and accumulate the total numbers of Vaxzevria and Janssen to compute the total numbers of vector vaccines per week. We scale this number down to our model's population size by dividing it through the total number of EU habitants and multiplicate it by the number of individuals in our model. We subsequently accumulate the vaccines within each 14-day interval $\mathcal{T}_i$ and divide this number by 14 to get the average number of vaccine doses inflow per vaccine and day. Thus, the inflow per day of each vaccine is constant within each interval $\mathcal{T}_i$ but varies across intervals and vaccines. As a results, we get the stepwise functions shown in Figure 7.

Overall, the inflow increases over time. This is due to the improvement of manufacturer infrastructure over the time course of the pandemic in the real world and the constantly high demand for vaccines.

4.2 Deterministic simulations

We use Python and mainly its libraries libSBML (Bornstein et al., 2008) and AMICI (Fröhlich et al., 2021) to implement our models. pyPESTO (Schälte et al., 2021) is our main tool for optimization. To minimize the optimization problem, we use the L-BFGS-B algorithm

Total available vaccine doses in million
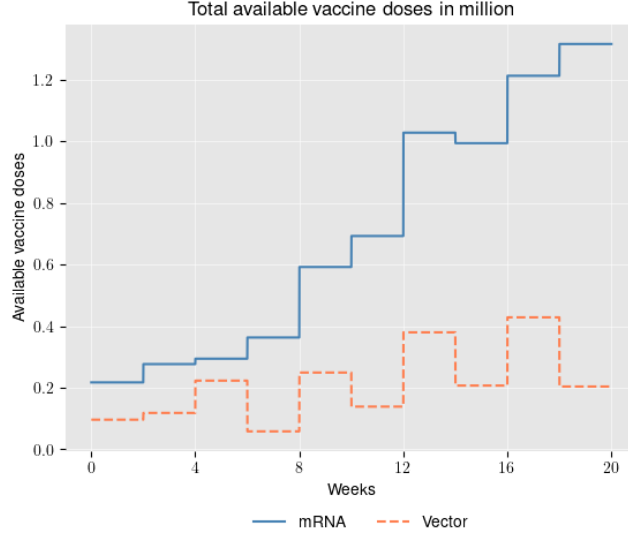
Note: The total inflow of mRNA and vector vaccines is accumulated for each 2-week decision period and equally distributed across days. Real-world numbers are scaled down by a population size adjustment to account for the population size of our model.

Figure 7: Time course of exogenous vaccine inflow

(Zhu et al., 1997) for which pyPESTO uses Scipy's (Virtanen et al., 2020) implementation. For each optimization we run a multi-start using 50 starts and choose the corresponding vaccination strategy that minimizes the objective. We provide waterfall plots for the piecewise constant and the spline multi-start optimization within Appendix A.2.3 in Figure 21a and Figure 21b. For each start, we draw uncorrelated start parameters $\theta_{l,i} \sim \mathcal{U}(0,1)$. In the case of Pareto optimal constraints, we only accept a starting vector Θ if the Pareto constraints $C.5$ and $C.6$ are satisfied. Otherwise, we reject it and draw a new sample until 50 starts are reached.

Figure 8 provides a visualization of the number of deceased individuals using splines as vaccination channel. We show the results for the current strategy (first row), the Pareto optimal strategy (second row), and the unrestricted strategy (third row) and split up the numbers of deceased individuals with respect to their country of origin. For all strategies, there are far more deaths in country B, which is due to the more infectious mutant that has been present only in country B at $t = 0$. Both optimized strategies outperform the current strategy, which seems to be plausible given that the optimized strategies take the model states into account and the current strategy only follows a pre-allocation. The unrestricted

31

strategy also outperforms the Pareto optimal strategy, which results from the nature of the optimization specification, since they are essentially the same optimization problem, but the Pareto parameter space is restricted by the two Pareto conditions $C.5$ and $C.6$.
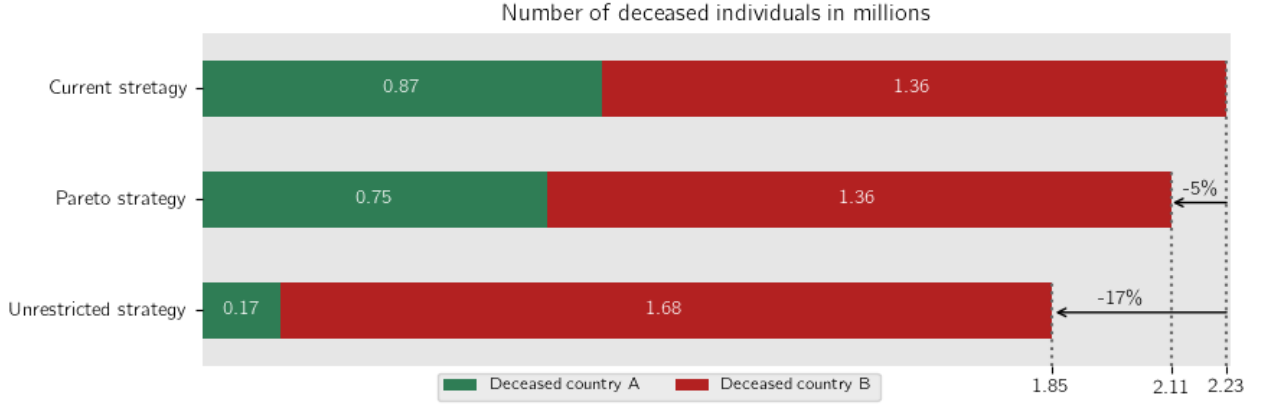

Note: The numbers within the boxes indicate the number of deceased individuals in millions with respect to the respective country and strategy. Numbers at the x-axis represent the total number of deceased individuals within one country. The percentage numbers indicate the change relative to the optimal strategy, e.g. -5% indicates that by implementing the Pareto strategy 5% fewer individuals died in comparison to the current strategy.

Figure 8: Number of deceased individuals by country (splines)

The unrestricted strategy yields a reduction in deaths by around 17% relative to the current strategy. However, given full knowledge of the outcome, policymakers in country B would not agree to implement this strategy due to the increase of around 320,000 deaths in country B. The Pareto strategy yields the same number of death cases in country B as the current strategy but at the same time, death cases in country A can be reduced by around 130,000, yielding an overall improvement of around 5% relative to the current strategy. Thus, the Pareto optimal strategy is more likely to be approved by both countries given that it makes none of them worse but one country better off than the current strategy.

Figure 9 depicts the vaccine inflow of each country dependent on the vaccination strategy. We show the results for the three strategies (columns) and split up the results by countries (rows). Due to equi-allocation, the vaccine inflow of the current strategy is 50% of the total vaccine inflow shown in Figure 7. Most strikingly, the unrestricted strategy assigns vaccines to country B only between the 5th and the 9th week as well as at the first and the last periods. The period between the 5th and the 9th week is where the number of infectious cases increases exponentially within country B, as can be seen in Figure 10.

The vaccine shortage in country B partly explains the large number of death cases in country B which we find in Figure 8. On the contrary, the Pareto strategy assigns much more doses to country B, especially at the end of the decision horizon. As seen in Figure 8, this comes with the cost of more deaths in country A compared to the unrestricted strategy but the benefit of an overall Pareto improvement compared to the current strategy.
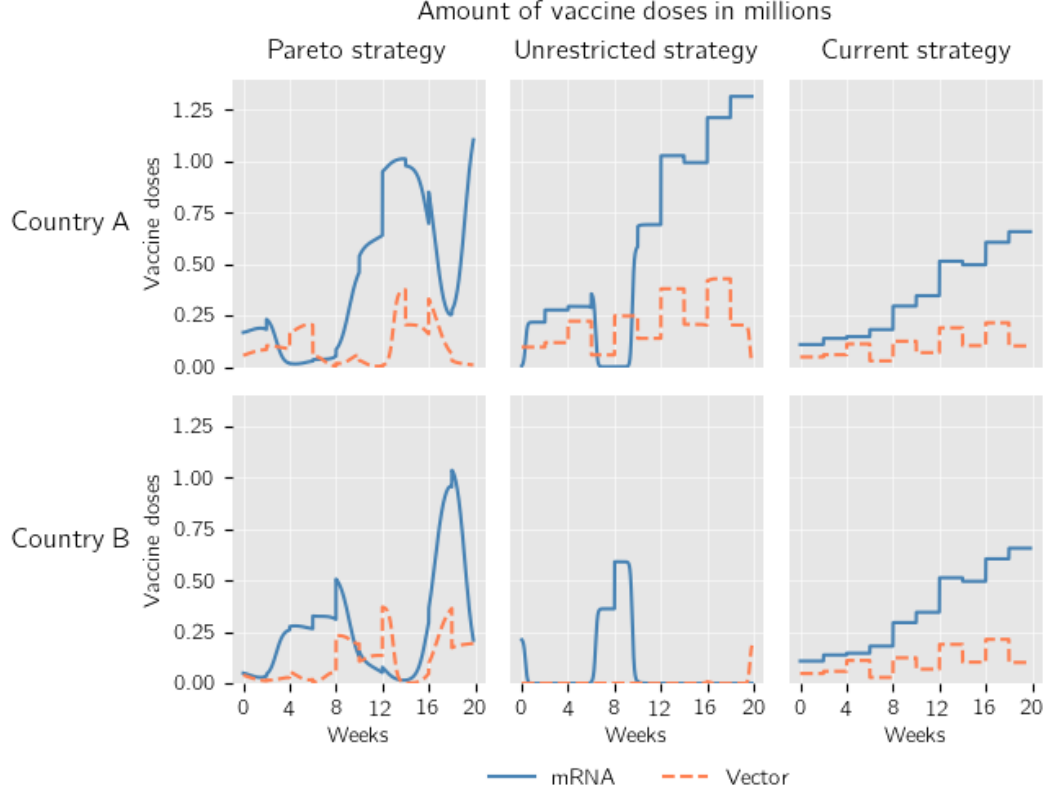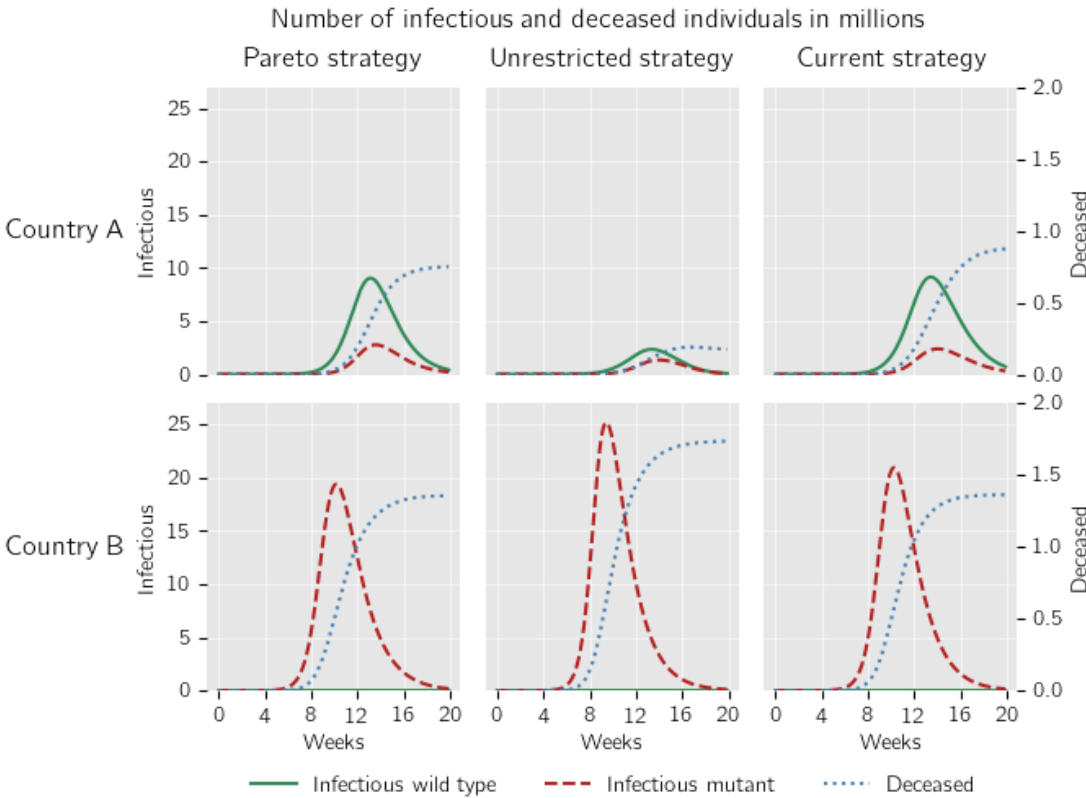

Note: Every column represents one vaccination strategy and every row represents one country. Both vaccines are indicated by the colors that are used throughout the paper. Every curve is the product of a piecewise constant vaccine inflow and a spline. Thus, the lines appear to be discontinuous piecewise polynomials.

Figure 9: Number of allocated vaccine doses (splines)

With respect to the current strategy, we observe that the optimized strategies are different from the current strategy. This is highlighted within Figure 20 in Appendix A.2.2, where we plot the course of the functions f_l. Figure 20 also shows that the time courses of f_1 and f_2 show similar shapes indicating that vaccines are rather allocated as a bundle.

In Figure 10, we trace out the trajectories of the number of infectious and deceased individuals according to the respective strategies (columns) and countries (rows). Regardless of the strategy, only the mutant spreads in country B. This is due to the initial allocation

of ten mutant infected individuals in country B and ten wild type infected individuals in country A as well as the higher infectiousness of the mutant. The higher infectiousness of 20% prevents the wild type from spreading in country B via cross-border infections. On the contrary, country A has to deal with both variants due to the cross-border infections. The unrestricted strategy can keep infections in country A below 2 million, whereas the Pareto strategy and the current strategy yield more than 7 million cases.

Note: Every column represents one vaccination strategy and every row represents one country. Every vaccine is indicated by its color that is used throughout the paper. The left y-axis is used for the number of infectious individuals (solid green and dashed red curves). The right y-axis corresponds to the number of deceased individuals (dotted blue line). Both viruses are associated with the color we have used throughout the paper.

Figure 10: Number of infectious individuals (splines)

4.3 Policy test with stochastic model

We test the deterministically derived strategies within the stochastic set-up from Section 2.2 to examine how they perform in an uncertain world where infections, recoveries, and deaths do not follow pre-determined patterns. We generate 500 samples per strategy by running Algorithm 1. Unfortunately, we cannot simulate the algorithm with a set of random variables and test every strategy for this set and compare the results with a counterfactual interpretation. This is due to the nature of the problem. The means of the Poisson random variables in Equation (7) depend on the system's state and therefore the magnitude of randomness changes with the strategies, making counterfactual interpretations of the vaccination strategies as a whole unfeasible.

Figure 11 depicts the histograms of the number of deaths clustered by the three strategies. The average number of deceased individuals is between 0.78 and 0.95 million higher as in the respective deterministically derived strategies. However, we observe on average the same order as for the deterministic case. The unrestricted strategy yields the fewest deaths whereas most deaths are observed for the current strategy. We plot the joint distribution of the deaths
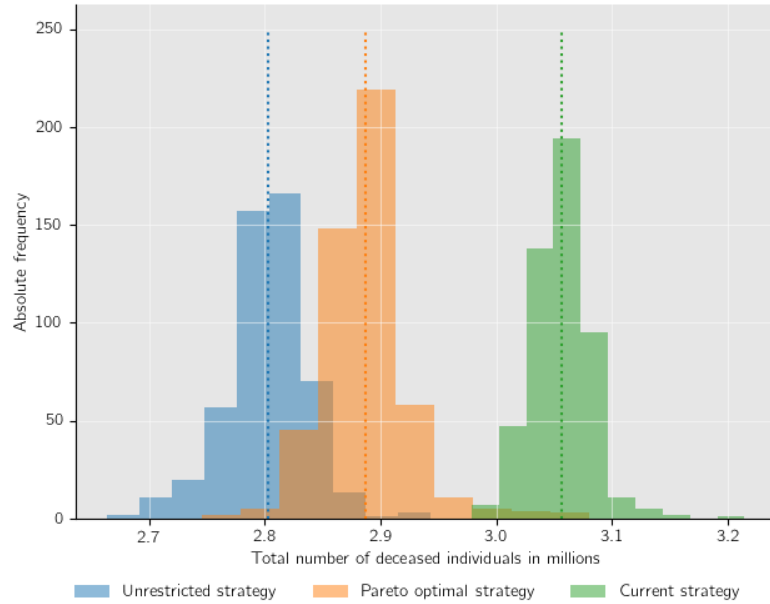

Note: Dotted lines are sample means. The total number of deceased individuals of a strategy is the sum of the respective number of deaths in country A and country B. We draw 500 samples per strategy.

Figure 11: Stochastically observed frequencies (splines)

split up by country and the respective marginal histograms in Figure 24 in Appendix A.2.4.

In Figure 12, we explore how the number of infectious individuals varies within the samples. The course of infectious individuals of the unrestricted strategy in country B captures the deterministic numbers well. Within the other figures, the case numbers seem to be higher within the stochastic model, which is in line with the increased number of deaths observed in Figure 11.
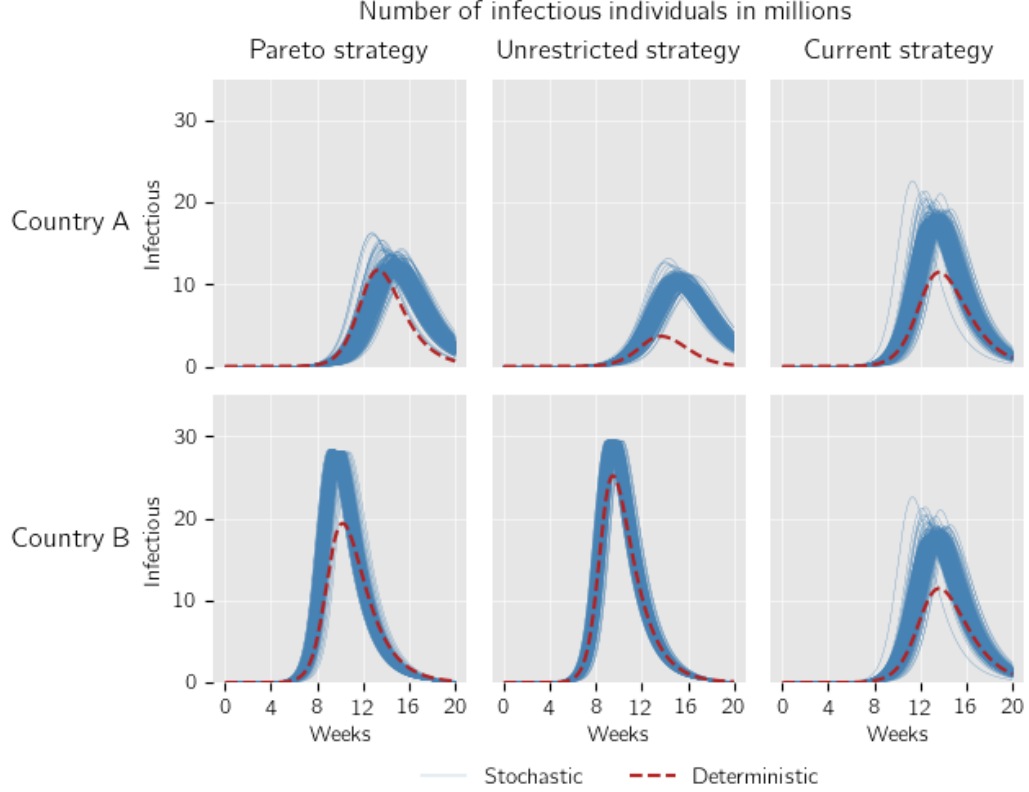
Note: Every column represents one vaccination strategy and every row represents one country. The thin blue lines depict all 500 simulations of the stochastic algorithm using the respective strategy. The dashed red depicts the respective infections within the deterministic model.

Figure 12: Number of infectious individuals using stochastic simulations (splines)

5   Conclusion

Our research aims to identify potential improvements in the population size based EU vaccination policy against the COVID-19 pandemic such that deaths across countries can be minimized. We propose a deterministic SIRD compartment model with two countries and two vaccines to examine the effect of optimal strategies compared to the current EU strat-

egy. We calibrate our model with parameters from the literature and the real-world vaccine inflow of the COVID-19 vaccines. We construct the vaccination channels via piecewise constant functions and splines. We examine one case where we impose further restrictions on the optimal vaccine allocation and another case where we constrain the results to be an improvement for each country. We simulate the models numerically and validate the optimal strategies derived from the deterministic model in a stochastic extension to our model.

Our results show that the optimal derived vaccination strategies differ from the current EU strategy, which could indicate that more complex vaccination policies can lower the number of death cases caused by the pandemic. Enhancing the robustness of our results, we qualitatively find highly similar results using piecewise constant and spline vaccination channels. Leaving aside country-specific interests, it appears that assigning most vaccine doses to one country can be as much as 17% beneficial, leading to a reduction of approximately 80% fewer deaths within this country. The other country then experiences a substantial increase in deaths of about 23%. But since the decrease in the number of cases in the first country is substantially lower, this leads to an overall decrease in the number of deaths. However, policymakers of the second country would not be willing to agree to this policy due to the higher case numbers. We find that imposing additional Pareto constraints yields an overall improvement of 5% in comparison to the current strategy but an overall deterioration in comparison to the unrestricted optimal strategy. The Pareto optimal strategy derived by the model assigns just enough vaccine doses to the second country such that it has the same case numbers as for the baseline EU strategy. However, the first country is better off, leading to an overall improvement of the Pareto strategy in comparison to the current strategy. Since both countries are not worse off, they have no incentive to vote against the Pareto optimal strategy, making it more likely to be implemented in practice. Stochastic simulations yielded higher death numbers but underlined the general findings with respect to the efficiency of the strategies.

In ongoing work, we pursue two avenues for further improvement. First, we implement neural networks as the third channel of vaccine allocation. The piecewise constant approach and the splines do not yield constructive vaccination strategies since we do not link the vaccine allocation directly to the states of the model. As inputs for the neural network model,

we use states and parameters that could be (at least approximately) observed in the real world, such as the current infected case numbers, the change in infected case numbers, and the reproduction number. Due to the linkage of vaccine allocation output to the model states, an optimal allocation in this scenario is transferable to the real world in the sense that the real-world vaccination strategy can be adjusted according to the output of the neural network, given the real-world's state. Second, we plan to incorporate further compartments that account for different age structures of countries. Adding further age-dependent compartments may help us to understand how vaccination strategies must be adapted according to country-specific demographics. We especially aim to focus on the implications of child vaccinations.

In addition, it might be worth examining how the dynamics of the model change after including testing and quarantines. We are particularly interested in examining how testing and vaccinations can be optimally exploited together or whether tests can even substitute for vaccinations up to a certain degree. Moreover, our analysis does not account for non-death related disutilities, like physical long-term damage caused by infection. A modified objective that takes long-term measures into account could help to address this issue.

Our findings regarding the unrestricted optimization trace out a crucial dilemma for policy makers of supranational institutions, such as the European Union, when it comes to choosing a vaccination strategy for the current COVID-19 pandemic. On the one hand, choosing the overall number of death cases as objective measure seems to be plausible. On the other hand, the supranational policymakers cannot outweigh the disutility of one country with the benefits of another country. However, our findings concerning the Pareto optimality indicate that given the current strategy, a Pareto improvement might be possible to achieve and for policymakers to apply, if further research is conducted.

References

Abu-Raddad, L. J., Chemaitelly, H., and Butt, A. A. (2021). Effectiveness of the BNT162b2 COVID-19 vaccine against the B.1.1.7 and B.1.3.51 variants. *The New England Journal of Medicine.*

Baud, D., Qi, X., Nielsen-Saines, K., Musso, D., Pomar, L., and Favre, G. (2020). Real estimates of mortality following COVID-19 infection. *The Lancet*, 20(7):773.

Bertsimas, D., Ivanhoe, J. K., Jacquillat, A., Li, M. L., Previero, A., Lami, O. S., and Bouardi, H. T. (2020). Optimizing vaccine allocation to combat the COVID-19 pandemic. *medRxiv Working Paper.*

Biontech (2021). mRNA vaccines to address the COVID-19 pandemic. `https://biontech.de/covid-19-portal/mrna-vaccines`, Last accessed on 2021-07-12.

Bornstein, B. J., Keating, S. M., Jouraku, A., and Hucka, M. (2008). LibSBML: An API library for SBML. *Bioinformatics*, 24(6):880–881.

Byambasuren, O., Cardona, M., Bell, K., Clark, J., McLaws, M.-L., and Glasziou, P. (2020). Estimating the extent of asymptomatic COVID-19 and its potential for community transmission: Systematic review and meta-analysis. *Official Journal of the Association of Medical Microbiology and Infectious Disease Canada*, 5(4):223–234.

Callaway, E. (2021). Delta coronavirus variant: Scientists brace for impact. *Nature*, 595:17–18.

CDC (2021). Key things to know about COVID-19 vaccines. `https://www.cdc.gov/coronavirus/2019-ncov/vaccines/keythingstoknow.html`, Last accessed on 2021-07-12.

Davies, N. G., Jarvis, C. I., Edmunds, W. J., Jewell, N. P., Diaz-Ordaz, K., and Keogh, R. H. (2021). Increased mortality in community-tested cases of SARS-CoV-2 lineage B.1.1.7. *Nature*, 593(7858):270–274.

Deb, P., Furceri, D., Ostry, J. D., and Tawk, N. (2020). The economic effects of COVID-19 containment measures. *IMF Working Papers.*

ECDC (2021a). COVID-19 situation update worldwide, as of week 27. `https://www.ecdc.europa.eu/en/geographical-distribution-2019-ncov-cases`, Last accessed on 2021-07-19.

ECDC (2021b). Data on COVID-19 vaccination in the EU/EEA. `"https://opendata.ecdc.europa.eu/covid19/vaccine_tracker/xlsx/data.xlsx"`, Last accessed on 2021-07-12.

ECDC (2021c). SARS-CoV-2 variants of concern as of 15 July 2021. `https://www.ecdc.europa.eu/en/covid-19/variants-concern`, Last accessed on 2021-07-19.

Emary, K. R. W., Golubchik, T., Aley, P. K., Ariani, C. V., et al. (2021). Efficacy of chadox1 nCoV-19 (azd1222) vaccine against SARS-CoV-2 variant of concern. *The Lancet*, 397(10282):1351–1362.

European Commission (2021a). Questions and answers on COVID-19 vaccination in the EU. `https://ec.europa.eu/info/live-work-travel-eu/coronavirus-response/safe-covid-19-vaccines-europeans/questions-and-answers-covid-19-vaccination-eu_en`, Last accessed on 2021-07-13.

European Commission (2021b). Safe COVID-19 vaccines for Europeans. `"https://ec.europa.eu/info/live-work-travel-eu/coronavirus-response/safe-covid-19-vaccines-europeans_en"`, Last accessed on 2021-07-13.

Fröhlich, F., Weindl, D., Schälte, Y., Pathirana, D., Paszkowski, Ł., Lines, G. T., Stapor, P., and Hasenauer, J. (2021). AMICI: High-performance sensitivity analysis for large ordinary differential equation models. *Bioinformatics*. btab227.

Gabler, J., Raabe, T., Röhrl, K., and von Gaudecker, H.-M. (2021). The effectiveness of strategies to contain SARS-CoV-2: Testing, vaccinations, and NPIs. *arXiv Working Paper*.

Gartlehner, G., Hansen, R. A., Nissman, D., Lohr, K. N., and Carey, T. S. (2006). *Criteria for distinguishing effectiveness from efficacy trials in systematic reviews*. Agency for Healthcare Research and Quality, Rockville, MD.

Gillespie, D. T. (1977). Exact stochastic simulation of coupled chemical reactions. *The Journal of Physical Chemistry*, 81(25):2340–2361.

Gillespie, D. T. (2001). Approximate accelerated stochastic simulation of chemically reacting systems. *The Journal of Chemical Physics*, 115(4):1716–1733.

Harris, R. J., Hall, J. A., Zaidi, A., Andrews, N. J., Dunbar, J. K., and Dabrera, G. (2021). Impact of vaccination on household transmission of SARS-COV-2 in England. *medRxiv Working Paper*.

Hindmarsh, A. C., Brown, P. N., Grant, K. E., Lee, S. L., Serban, R., Shumaker, D. E., and Woodward, C. S. (2005). SUNDIALS: Suite of nonlinear and differential/algebraic equation solvers. *ACM Transactions on Mathematical Software (TOMS)*, 31(3):363–396.

Hindmarsh, A. C., Serban, R., and Reynolds, D. R. (2021). User Documentation for CVODE v5.7.0 (SUNDIALS v5.7.0). Technical Report.

Hui, D. S., Azhar, E. I., Madani, T. A., Ntoumi, F., Kock, R., Dar, O., Ippolito, G., Mchugh, T. D., Memish, Z. A., Drosten, C., et al. (2020). The continuing 2019-nCoV epidemic threat of novel coronaviruses to global health - The latest 2019 novel coronavirus outbreak in Wuhan, China. *International Journal of Infectious Diseases*, 91:264–266.

Jongeneelen, M., Kaszas, K., Veldman, D., Huizingh, J., van der Vlugt, R., Schouten, T., Zuijdgeest, D., Uil, T., van Roey, G., Guimera, N., et al. (2021). Ad26. COV2. S elicited neutralizing activity against delta and other SARS-CoV-2 variants of concern. *bioRxiv*.

Matrajt, L., Eaton, J., Leung, T., and Brown, E. R. (2021). Vaccine optimization for COVID-19: Who to vaccinate first? *Science Advances*, 7(6):eabf1374.

Miles, D., Stedman, M., and Heald, A. (2020). Living with COVID-19: balancing costs against benefits in the face of the virus. *National Institute Economic Review*, 253:R60–R76.

Mullard, A. (2020). COVID-19 vaccine development pipeline gears up. *The Lancet*, 395(10239):1751–1752.

Nasreen, S., He, S., Chung, H., Brown, K. A., Gubbay, J. B., Buchan, S. A., Wilson, S. E., Sundaram, M. E., Fell, D. B., Chen, B., et al. (2021). Effectiveness of COVID-19 vaccines against variants of concern. *medRxiv Working Paper*.

Oliver, S. E. (2021a). The advisory committee on immunization practices' interim recommendation for use of Janssen COVID-19 vaccine. *Morbidity and Mortality Weekly Report*, 70(9):329–332.

Oliver, S. E. (2021b). The advisory committee on immunization practices' interim recommendation for use of Moderna COVID-19 vaccine. *Morbidity and Mortality Weekly Report*, 69(5152):1653–1656.

Poisson, S. D. (1835). Recherches sur la probabilité des jugements, principalement en matiére criminelle. *Comptes-Rendus Hebdomadaires des Séances de l'Académie des Sciences*, 1:473–494.

Polack, F. P., Thomas, S. J., Kitchin, N., Absalon, J., Gurtman, A., Lockhart, S., Perez, J. L., Marc, G. P., Moreira, E. D., Zerbini, C., et al. (2020). Safety and efficacy of the BNT162b2 mRNA COVID-19 vaccine. *The New England Journal of Medicine*.

Prüß, B. M. (2021). Current state of the first COVID-19 vaccines. *Vaccines*, 9(1):30–31.

Robert Koch Institut (2021). Epidemiologischer Steckbrief zu SARS-CoV-2 und COVID-19. `https://www.rki.de/DE/Content/InfAZ/N/Neuartiges_Coronavirus/Steckbrief.`, Last accessed on 2021-07-12.

Roy, S. (2020). COVID-19 reinfection: Myth or truth? *SN Comprehensive Clinical Medicine*, 2(6):710–713.

Runge, C. (1901). Über empirische Funktionen und die Interpolation zwischen äquidistanten Ordinaten. *Zeitschrift für Mathematik und Physik*, 46(20):224–243.

Sadoff, J., Gray, G., Vandebosch, A., Cárdenas, V., Shukarev, G., Grinsztejn, B., Goepfert, P. A., Truyers, C., Fennema, H., Spiessens, B., et al. (2021). Safety and efficacy of single-dose Ad26. COV2. S vaccine against COVID-19. *The New England Journal of Medicine*, 384(23):2187–2201.

Schälte, Y., Vanhoefer, J., Fröhlich, F., and Stapor, P. (2021). pyPESTO - Parameter estimation toolbox for Python.

Sheikh, A., McMenamin, J., Taylor, B., and Robertson, C. (2021). SARS-CoV-2 Delta VOC in Scotland: Demographics, risk of hospital admission, and vaccine effectiveness. *The Lancet*, 397(10293):2461–2462.

Skelly, D. T., Harding, A. C., Gilbert-Jaramillo, J., Knight, M. L., Longet, S., Brown, A., Adele, S., Adland, E., Brown, H., Team, M. L., et al. (2021). Vaccine-induced immunity provides more robust heterotypic immunity than natural infection to emerging SARS-CoV-2 variants of concern. *Research Square Preprint*.

Statistisches Bundesamt (2017). Ankünfte, Übernachtungen und durchschnittliche Aufenthaltsdauer in Beherbergungsbetrieben: Deutschland, Jahre, ausgewählte Herkunftsländer der Gäste. *Ergebnisse der Monatserhebung im Tourismus*.

Stowe, J., Andrews, N., Gower, C., Gallagher, E., Utsi, L., and Simmons, R. (2021). Effectiveness of COVID-19 vaccines against hospital admission with the Delta (B. 1.617. 2) variant. *The New England Journal of Medicine*.

Tenforde, M. W. (2021). Effectiveness of Pfizer-BioNTech and Moderna vaccines against COVID-19 among hospitalized adults aged $\geq$ 65 years. *Morbidity and mortality weekly report*, 70(18):674–679.

Tuite, A. R., Zhu, L., Fisman, D. N., and Salomon, J. A. (2021). Alternative dose allocation strategies to increase benefits from constrained COVID-19 vaccine supply. *Annals of Internal Medicine*, 174(4):570–572.

Virtanen, P., Gommers, R., Oliphant, T. E., Haberland, M., Reddy, T., Cournapeau, D., Burovski, E., Peterson, P., Weckesser, W., Bright, J., van der Walt, S. J., et al. (2020). SciPy 1.0: Fundamental algorithms for scientific computing in Python. *Nature Methods*, 17:261–272.

Voysey, M., Clemens, S. A. C., Madhi, S. A., Weckx, L. Y., Folegatti, P. M., Aley, P. K., Angus, B., Baillie, V. L., Barnabas, S. L., Bhorat, Q. E., et al. (2021). Single-dose administration and the influence of the timing of the booster dose on immunogenicity and efficacy of ChAdOx1 nCoV-19 (AZD1222) vaccine: A pooled analysis of four randomised trials. *The Lancet*, 397(10277):881–891.

Wu, Z. and McGoogan, J. M. (2020). Characteristics of and important lessons from the coronavirus disease 2019 (COVID-19) outbreak in China: Summary of a report of 72,314 cases from the Chinese Center for Disease Control and Prevention. *Jama*, 323(13):1239–1242.

Zhu, C., Byrd, R. H., Lu, P., and Nocedal, J. (1997). Algorithm 778: L-BFGS-B: Fortran subroutines for large-scale bound-constrained optimization. *ACM Transactions on Mathematical Software*, 23(4):550–560.

A   Appendix

A.1   Sensitivity

In this section we examine the sensitivity of our model with respect to certain parameters. We use 10-start multi-start optimizations for the Pareto optimal and the unrestricted strategy. We use 10 starts instead of 50, as in the main section, to reduce the computational costs. The results should therefore not be compared to the results from the main section with regard to absolute numbers. However, we can use the results of the sensitivity analysis to learn about the influence of parameter changes on the death cases.

A.1.1   Sensitivity of cross-border enocunters

In Figure 13, we examine the influence of the parameter that determine cross-border encounters on the number of deaths. Recall that the distance function $b(d(A, B))$ maps to the unit interval and b is strictly decreasing such that large distances between countries result in fewer cross-border encounters. From Equation (31), we have derived that $b(d(A, B)) \to 1$ means that cross-border encounters are equally likely as within-country encounters and that $b(d(A, B)) \to 0$ means that cross-border encounters become unlikely.
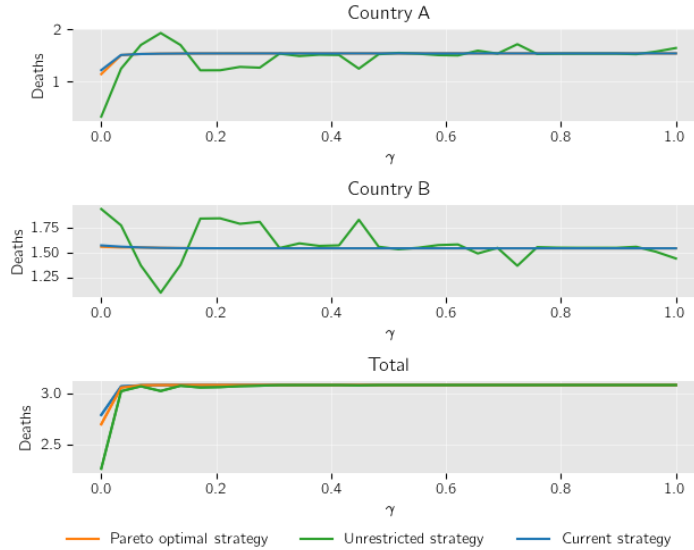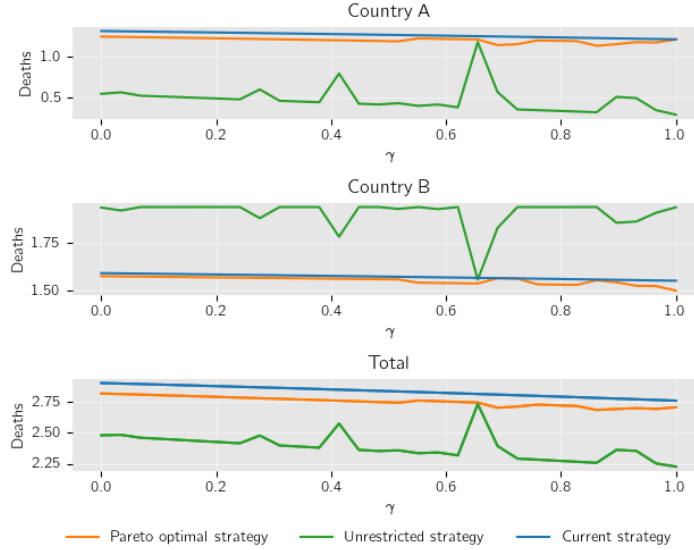

Note: To compute the optimized values of the Pareto strategy and the unrestricted strategy a multi-start with 10 runs has been conducted.

Figure 13: Sensitivity with respect to the distance measure

We see as major takeaway from Figure 13 that the optimal strategies only outperform the current strategy for low values of $b(d(A, B))$. This could indicate that no improvement is possible, if cross-border encounters happen frequently. This might be explained by the fact that for high values of $b(d(A, B))$, individuals are likely to become infected from individuals of both countries such that the allocation of a fixed amount of vaccine doses cannot protect a certain country. This seems plausible and we see it as a proof of concept. However, simulations using more multi-starts might be necessary to fully examine the patterns.

A.1.2 Sensitivity of the mutant infectiousness

We trace out the effect of the infectiousness of the mutant type in Figure 14. As expected, the number of deaths increases with a more infectious mutant. Most strikingly, it seems that there is only a corridor around the interval $\eta \in [1.15, 1.4]$ where a Pareto improvement is possible. We hypothesize that for $\eta \in [1, 1.15)$ the effect of the higher mutant-infectiousness is negligible and for $\eta \in (1.4, 2]$ the effect is too severe, such that both countries experience a similar amount of deaths which cannot be influenced by the vaccine allocation. The latter is enhanced by the finding that for high values of η, country A and country B have similar numbers of deaths for the Pareto and the current strategy.
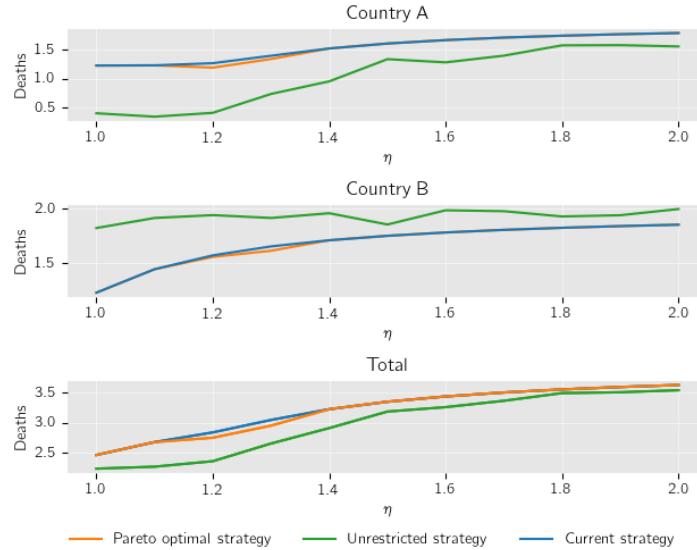
Note: To compute the optimized values of the Pareto strategy and the unrestricted strategy a multi-start with 10 runs has been conducted.

Figure 14: Sensitivity with respect to the parameter η

A.1.3 Sensitivity of virus spread prevention by vaccines

In Figure 15, we depict the sensitivity of number of deaths with respect to the parameter γ. Recall that γ is the reduction of transmitting the virus if an individual is vaccinated.

We find that the order of the strategies does not change over the whole range of γ. The number of death cases decreases nearly linear for the Pareto optimal and the current strategy but the decrease is rather small. This might be explained by the small number of individuals that become infected if they are vaccinated such that the influence of the not transmitting the virus does not influence the model severely. For the unrestricted optimal strategy, we observe peeks which could occur by chance due to the random draws of the starting values for the optimization. However, further research is needed to fully answer why these peeks occur.

Note: To compute the optimized values of the Pareto strategy and the unrestricted strategy a multi-start with 10 runs has been conducted.

Figure 15: Sensitivity with respect to the parameter γ

A.2 Supplementary results

We plot Figures that enhance our line of argumentation but would disturb the train of reading within the main section.

A.2.1 Piecewise constant results

Figure 16 provides a visualization of the core results using piecewise constant vaccination channels as functional form of f_l. The values do qualitatively not differ from the corresponding spline values depicted in the main text in Figure 8. Even the percentage improvements of the unrestricted and the Pareto strategy equal the numbers from the spline analysis. Since the current strategy is not affected by the type of the vaccination channel, it yields the exact same results as in Figure 8. For the optimized strategies, numbers are slightly shifted between countries, such that country A experiences between 10,000-30,000 more and country B fewer deaths. Figure 17 depicts the optimal doses of vaccine inflow using piecewise constant
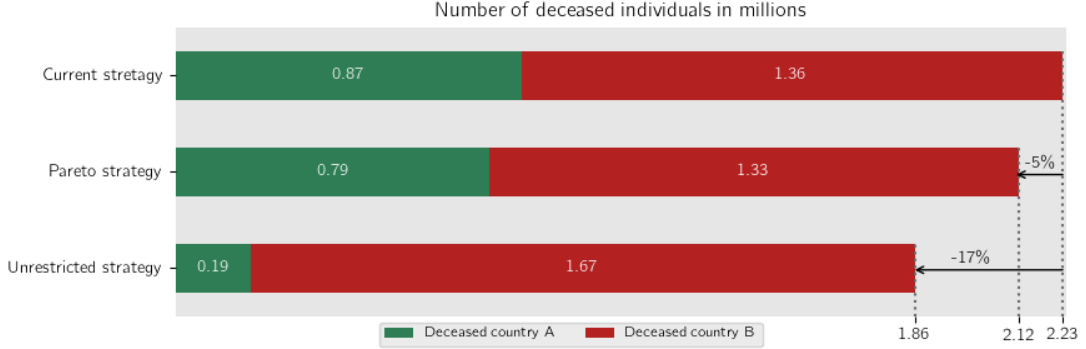
Note: The numbers within the boxes indicate the number of deceased individuals in millions with respect to the respective country and strategy. Numbers at the x-axis represent the total number of deceased individuals within one country. The percentage numbers indicate the change relative to the optimal strategy, e.g. −5% indicates that by implementing the Pareto strategy 5% less individuals died in comparison to the current strategy.

Figure 16: Number of deceased individuals by country (stepwise)

vaccination channels as functional form of f_l. As for the number of deceased individuals, the values do qualitatively not differ from the corresponding spline values depicted in the main text in Figure 9. Especially, we observe the pattern for the unrestricted strategy, which only assigns vaccine doses to country B between week 5 to 9.

In Figure 18, we trace out the trajectories of the number of infectious and deceased individuals according to the respective strategies (columns) and countries (rows). The values do not qualitatively differ form the corresponding spline values depicted in the main text in
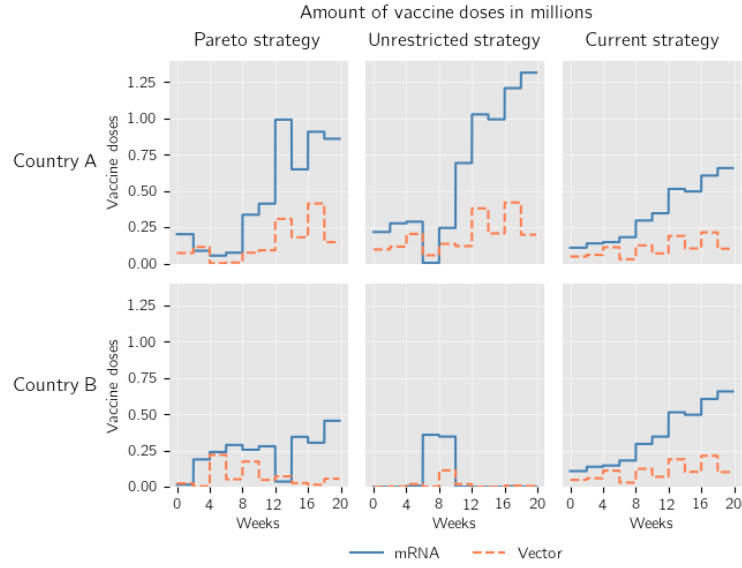
Note: Every column represents one vaccination strategy and every row represents one country. Both vaccines are indicated by their colors that are used throughout the paper. Every curve is the product of a piecewise constant vaccine inflow and a spline. Thus, the lines appear to be discontinuous piecewise polynomials.

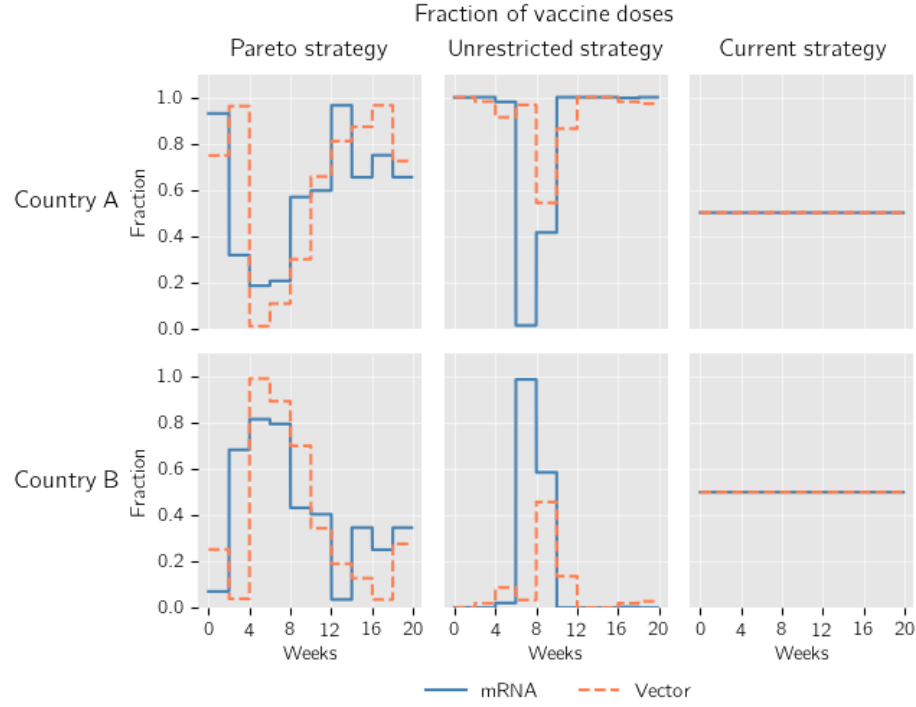Figure 17: Number of allocated vaccine doses (stepwise)

Figure 10.
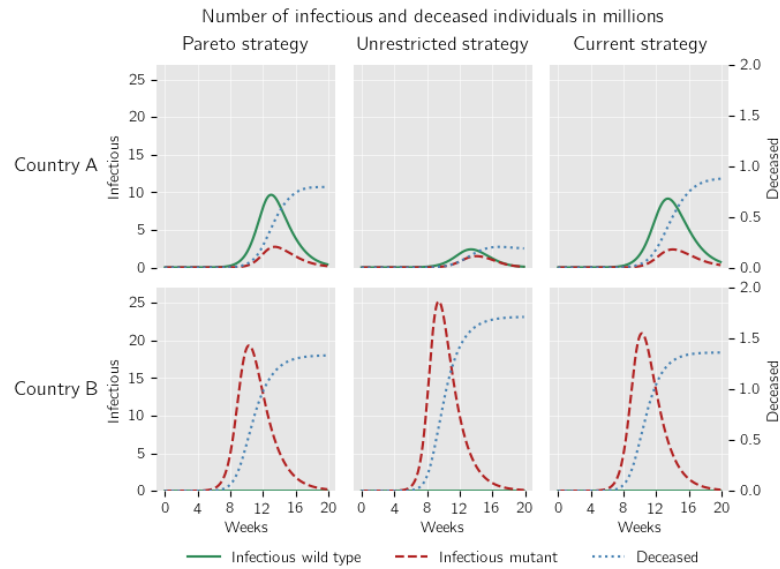
Note: Every column represents one vaccination strategy and every row represents one country. Every vaccine is indicated by its color that is used throughout the paper. The left y-axis is used for the number of infectious individuals (solid green and dashed red curves). The right y-axis corresponds to the number of deceased individuals (dotted blue line). Both viruses are associated with the color we have used throughout the paper.

Figure 18: Number of infectious individuals (stepwise)

A.2.2   Vaccination allocation fractions

Figure 19 depicts the course of f_l over the whole decison period using a piecewise vaccination channel. Figure 20 shows the respective values for the spline vaccination channels. The values are the quotient of the curve of the vaccine inflow in Figure 7 and the optimal total number of vaccine doses inflow in Figure 17 and Figure 9. The current strategy allocates half of the available vaccine doses to each country.

Note: Every column represents one vaccination strategy and every row represents one country. Both vaccines are indicated by their colors that are used throughout the paper.

Figure 19: Fractions of vaccines (stepwise)
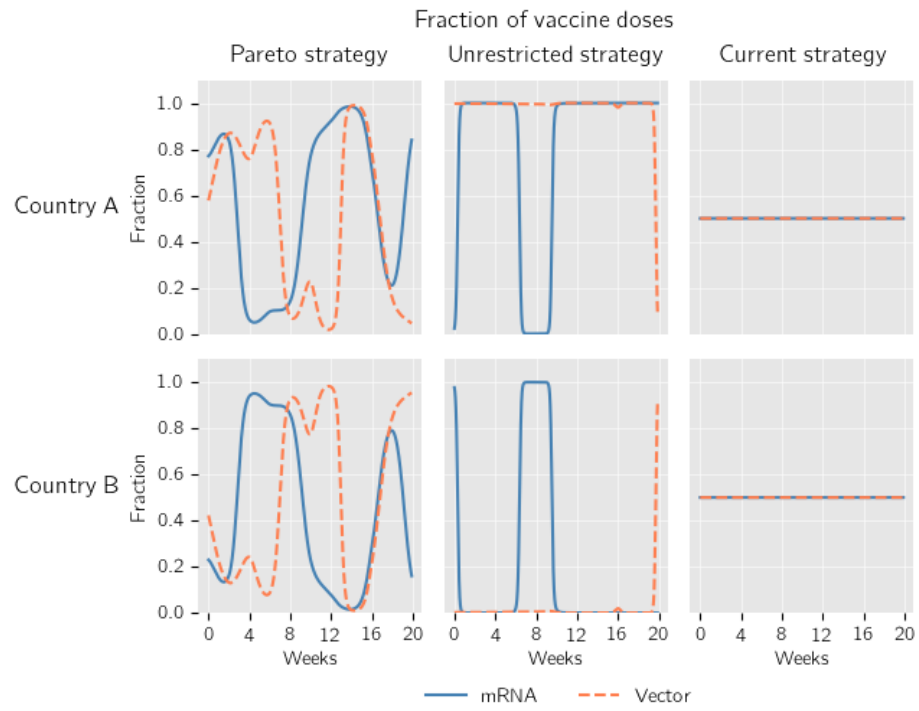
Note: Every column represents one vaccination strategy and every row represents one country. Both vaccines are indicated by their colors that are used throughout the paper.

Figure 20: Fractions of vaccines (splines)

A.2.3 Waterfall plots of optimization

Figure 21a and Figure 21b show the ordered 20 multi-start runs with the lowest optima of all 50 runs. We only show 20 runs to increase readability of the plot. We find that the descend of the ordered function values does not contain many jumps and the optimal values are obtained only once. Hence, it might be possible to find even lower values using more multi-start runs.

(a) Stepwise   (b) Splines
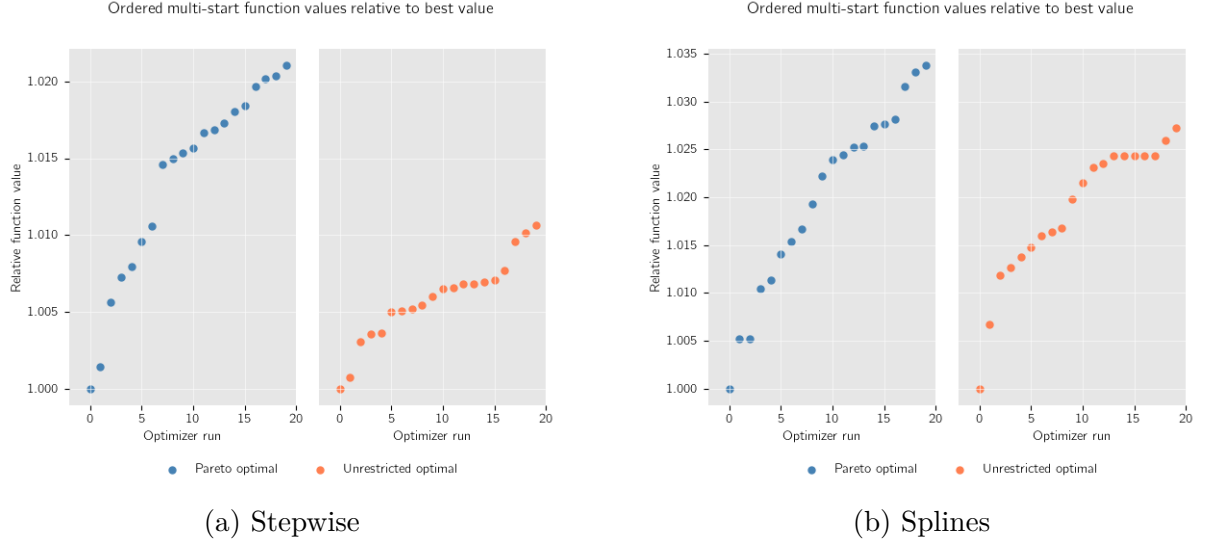
Note: Values are relative to the start yielding the lowest optimal minimum value. Only the best 20 starts are used to increase readability.

Figure 21: Waterfall plot of the 20 best multi-start runs (splines)

### A.2.4 Simulated distribution of number of deceased individuals

Figure 22 depicts the results for the number of deceased individuals using piecewise constant vaccination channels. We decided to remove it from the main text since the results resemble the results from the spline vaccination channel in Figure 11 in the main section.
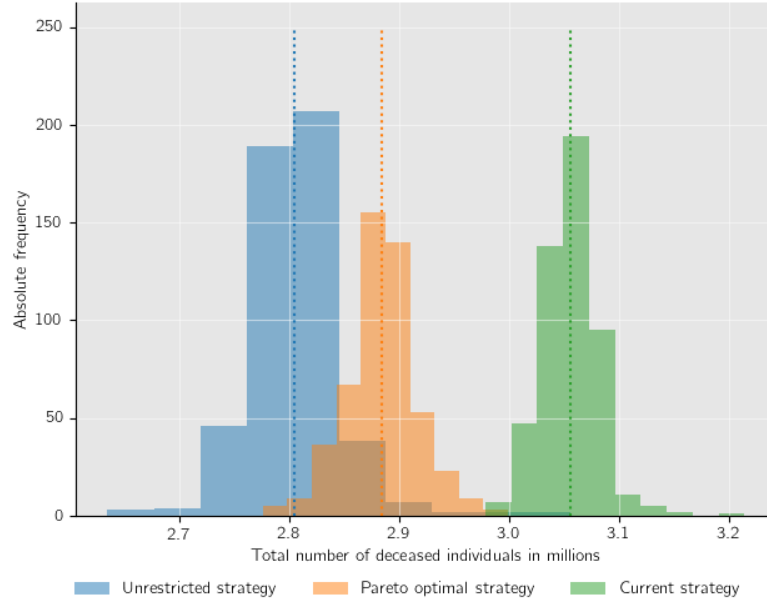
Note: Dotted lines are sample means. The total number of deceased individuals of a strategy is the sum of the respective number of deaths in in country A and country B. We draw 500 samples per strategy.

Figure 22: Stochastically observed frequencies (stepwise)

Figure 23 plots the total number of infectious individuals simulated using the stochastic model. We decided to remove it from the main text since the results resemble the results from the spline vaccination channel within Figure 12 in the main section.
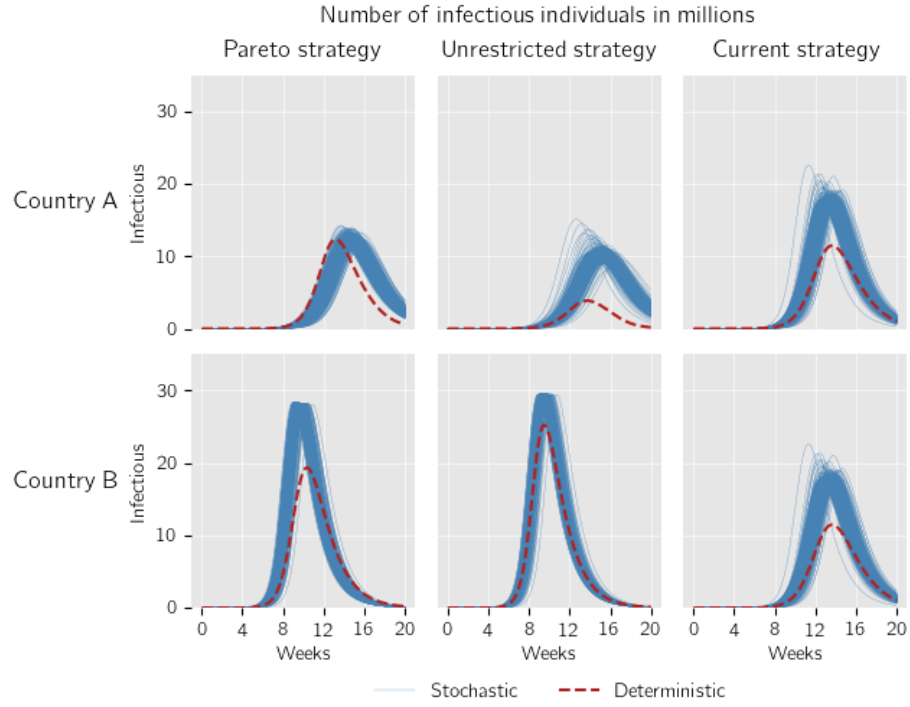
Note: Every column represents one vaccination strategy and every row represents one country. The thin blue lines depict all 500 simulations of the stochastic algorithm using the respective strategy. The dashed red depicts the respective infections within the deterministic model.

Figure 23: Number of infectious individuals using stochastic simulations (stepwise)

Figures 24 and 25 depict the 2-dimensional, as well as the marginal, histograms of the number of deceased individuals with respect to the countries. As for the results shown within the main section, the results are qualitatively highly similar. It is striking that for the unrestricted case, the case with the fewest deaths, points seem to fluctuate more random around the center point mass than for the Pareto optimal and the current strategy. For the current strategy and the optimal strategy the reasoning might be that, just by chance, some simulated pandemics result in overall more deaths and therefore both countries have increased numbers in death cases. However, the same reasoning could apply for the unrestricted strategy that shows no linear correlation. Further research is needed to examine if this patterns occurred randomly.
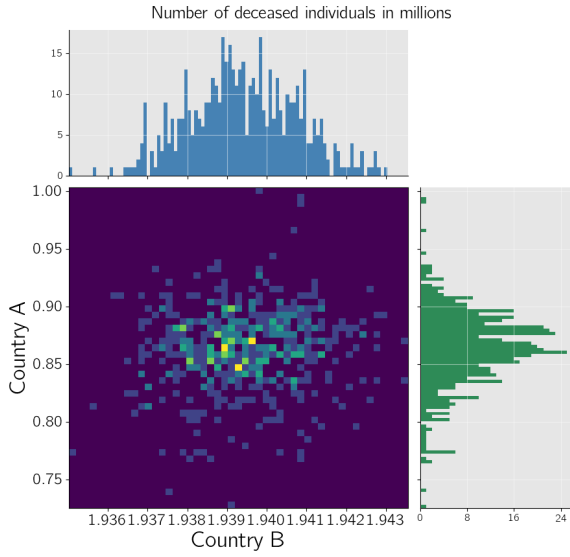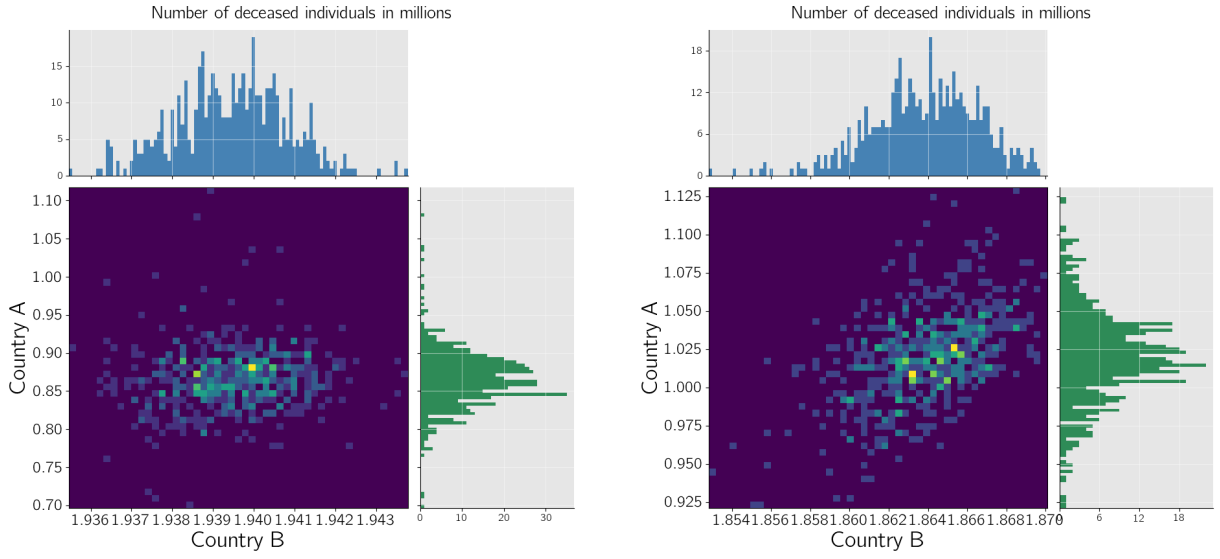
(a) Unrestricted strategy
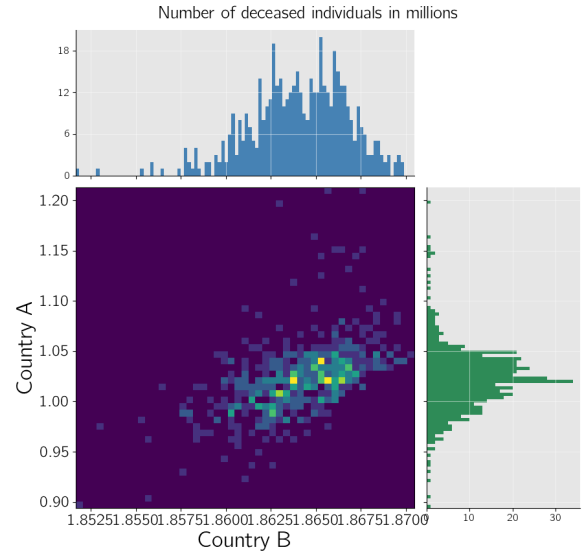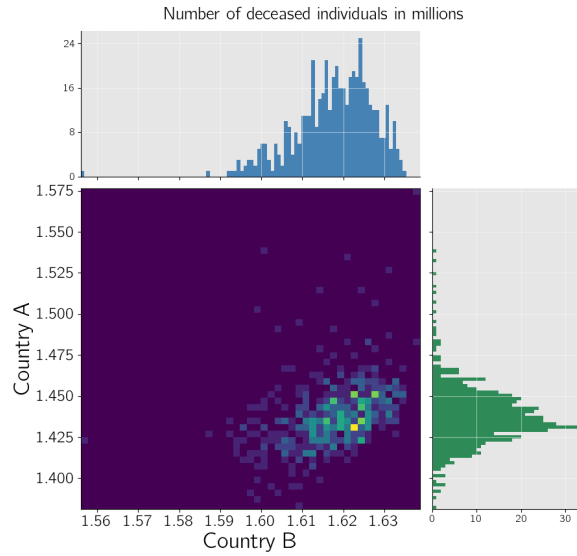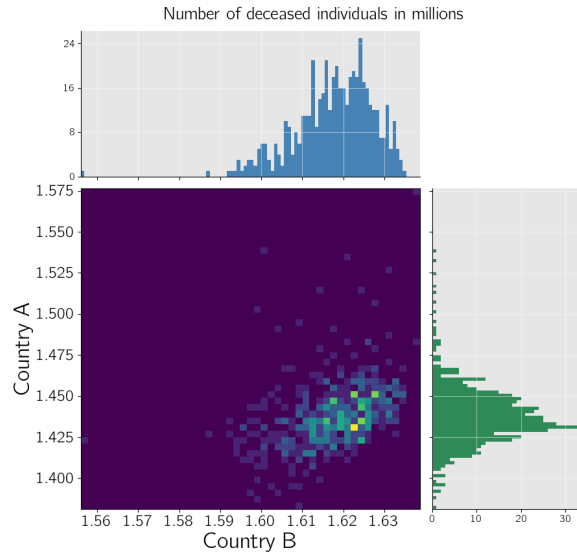
(b) Pareto optimal strategy

(c) Current strategy

Note: Purple temperature boxes indicate the joint frequencies. Histograms on top are the histograms corresponding to country B and histograms at the right-hand side are the histograms corresponding to country A. Histograms are computed using 500 simulations of the stochastic model using the Policies derived from splines.

Figure 24: Frequencies of number of deceased individuals (splines)

(a) Unrestricted strategy

(b) Pareto optimal strategy

(c) Current strategy

Note: Purple temperature boxes indicate the joint frequencies. Histograms on top are the histograms corresponding to country B and histograms at the right-hand side are the histograms corresponding to country A. Histograms are computed using 500 simulations of the stochastic model using the Policies derived from splines.

Figure 25: Frequencies of number of deceased individuals (stepwise)

A.3 Calculations and proofs

We provide calculations and proofs that enhance our line of argumentation but would disturb the train of reading within the main section.

A.3.1 Encounter probabilities

Using Bayes formula, we can rewrite the conditional probability as follows

$$\mathbb{P}_t(i_2 \in \mathcal{C}_t(X_S, C_j, F_2)|i_1 \in \mathcal{C}_t(\neg X_D, C_A)) \tag{31}$$
$$= \mathbb{P}_t(i_2 \in \mathcal{C}_t(\neg X_D, C_j, F_2)|i_1 \in \mathcal{C}_t(\neg X_D, C_A))$$
$$\cdot \mathbb{P}_t(i_2 \in \mathcal{C}_t(X_S)|i_1 \in \mathcal{C}_t(\neg X_D, C_A), i_2 \in \mathcal{C}_t(\neg X_D, C_j, F_2))$$
$$= \mathbb{P}_t(i_2 \in \mathcal{C}_t(\neg X_D, C_j, F_2)|i_1 \in \mathcal{C}_t(\neg X_D, C_A))$$
$$\cdot \mathbb{P}_t(i_2 \in \mathcal{C}_t(X_S)|i_2 \in \mathcal{C}_t(\neg X_D, C_j, F_2))$$

We use the relative number of susceptible individuals $\mathcal{C}_t(X_S, C_j, F_2)$ across all individuals of $\mathcal{C}_t(\neg X_D, C_j, F_2)$ as approximation of the probability at the second line of the right-hand side

$$\mathbb{P}_t(i_2 \in \mathcal{C}_t(X_S, F_2)|i_2 \in \mathcal{C}_t(\neg X_D, C_j, F_2)) = \frac{y_t(X_S, C_j, F_2)}{y_t(\neg X_D, C_j, F_2)}. \tag{32}$$

To account for the origin of i_1 within the first line of the right hand-side, we distinguish between the cases where $i_2 \in \mathcal{C}_t(C_A)$ and $i_2 \in \mathcal{C}_t(C_B)$. Assume that $i_2 \in \mathcal{C}_t(X_S, C_B, F_2)$. If there were no spatial effects to influence the cross-border encounter frequency we would use the unconditional probability

$$\mathbb{P}_t(i_2 \in \mathcal{C}_t(\neg X_D, C_j, F_2)) = \frac{y_t(\neg X_D, C_j, F_2)}{y_t(\neg X_D)}. \tag{33}$$

To account for the spatial effects, we introduce a penalty function $b : \mathbb{R}_+ \to [0, 1]$ that depends on the distances between both countries $d(A, B)$

$$\mathbb{P}_t(i_2 \in \mathcal{C}_t(\neg X_D, C_B, F_2)|i_1 \in \mathcal{C}_t(\neg X_D, C_A)) = \mathbb{P}_t(i_2 \in \mathcal{C}_t(\neg X_D, C_B, F_2)) \cdot b(d(A, B)), \tag{34}$$

yielding

$$\mathbb{P}_t(i_2 \in \mathcal{C}_t(X_S, C_B, F_2)|i_1 \in \mathcal{C}_t(\neg X_D, C_A)) = \frac{y_t(X_S, C_j, F_2)}{y_t(\neg X_D)} \cdot b(d(A, B)) \qquad (35)$$

A.3.2 Well-conditioning of the polynomial basis

The basis polynomials are defined by $B_1(t) = 2t^3 - 3t^2 + 1, B_2(t) = t^3 - 2t^2 + t, B_3(t) = -2t^3 + 3t^2$ and $B_4(t) = t^3 - t^2$. First note that $B_1(0) = 1$ and $B_2(0), B_3(0), B_4(0) = 0$. Furthermore, $B_1(1), B_2(1), B_4(1) = 0$ and $B_3(1) = 1$. We first compute the function values at the boundaries t_{i-1} and t_i.

$$\begin{aligned}
P_{l,i}(t_{i-1}) &= B_1(0)P_{l,i}(t_{i-1}) + B_2(0)(t_i - t_{i-1})P'_{l,i}(t_{i-1}) \\
&\quad + B_3(0)P_{l,i}(t_i) + B_4(0)(t_i - t_{i-1})P'_{l,i}(t_i) \\
&= 1 \cdot P_{l,i}(t_{i-1}) + 0 \cdot (t_i - t_{i-1})P'_{l,i}(t_{i-1}) \\
&\quad + 0 \cdot P_{l,i}(t_i) + 0 \cdot (t_i - t_{i-1})P'_{l,i}(t_i) \\
&= P_{l,i}(t_{i-1})
\end{aligned}$$

$$\begin{aligned}
P_{l,i}(t_i) &= B_1(1)P_{l,i}(t_{i-1}) + B_2(1)(t_i - t_{i-1})P'_{l,i}(t_{i-1}) \\
&\quad + B_3(1)P_{l,i}(t_i) + B_4(1)(t_i - t_{i-1})P'_{l,i}(t_i) \\
&= 0 \cdot P_{l,i}(t_{i-1}) + 0 \cdot (t_i - t_{i-1})P'_{l,i}(t_{i-1}) \\
&\quad + 1 \cdot P_{l,i}(t_i) + 0 \cdot (t_i - t_{i-1})P'_{l,i}(t_i) \\
&= P_{l,i}(t_i)
\end{aligned}$$

The derivatives of the basis polynomials are

$$B'_1(t) = 6t^2 - 6t$$
$$B'_2(t) = 3t^2 - 4t + 1$$
$$B'_3(t) = -6t^2 + 6t$$
$$B'_4(t) = 3t^2 - 2t$$

with $B_1(0)' = B_3(0)' = B_4(0)' = 0$ and $B_2(t)' = \frac{1}{t_i - t_{i-1}}$. Moreover, $B'_1(1)' = B_2(1)' =$

XIV

$B_3(1)' = 0$ and $B_4(1)' = \frac{1}{t_i - t_{i-1}}$. The derivative of the polynomial is simply

$$P'_{l,i}(t) = B'_1(t')P_{l,i}(t_{i-1}) + B'_2(t')(t_i - t_{i-1})P'_{l,i}(t_{i-1})$$
$$+ B'_3(t')P_{l,i}(t_i) + B'_4(t')(t_i - t_{i-1})P'_{l,i}(t_i)$$

and therefore

$$P'_{l,i}(t_{i-1}) = B'_1(0)P_{l,i}(t_{i-1}) + B'_2(0)(t_i - t_{i-1})P'_{l,i}(t_{i-1})$$
$$+ B'_3(0)P_{l,i}(t_i) + B'_4(0)(t_i - t_{i-1})P'_{l,i}(t_i)$$
$$= 0 \cdot P_{l,i}(t_{i-1}) + \frac{1}{t_i - t_{i-1}} \cdot (t_i - t_{i-1})P'_{l,i}(t_{i-1})$$
$$+ 0 \cdot P_{l,i}(t_i) + 0 \cdot (t_i - t_{i-1})P'_{l,i}(t_i)$$
$$= P'_{l,i}(t_{i-1})$$

and

$$P'_{l,i}(t_{i-1}) = B'_1(1)P_{l,i}(t_{i-1}) + B'_2(1)(t_i - t_{i-1})P'_{l,i}(t_{i-1})$$
$$+ B'_3(1)P_{l,i}(t_i) + B'_4(1)(t_i - t_{i-1})P'_{l,i}(t_i)$$
$$= 0 \cdot P_{l,i}(t_{i-1}) + 0 \cdot (t_i - t_{i-1})P'_{l,i}(t_{i-1})$$
$$+ 0 \cdot P_{l,i}(t_i) + \frac{1}{t_i - t_{i-1}} \cdot (t_i - t_{i-1})P'_{l,i}(t_i)$$
$$= P'_{l,i}(t_i).$$

A.3.3 Convergence in distribution

Theorem 1. $B\left(\frac{\tau}{dt}, a_j(y) \cdot dt\right) \xrightarrow{d} Po(a_j(y) \cdot \tau)$ *if* $dt \to 0$.

Proof. Let p_n be a sequence with $\lim_{n \to \infty} p_n = 0$. We first show that if $\lambda' = n \cdot p_n$ is constant, $n \to \infty$ and $p_n \to 0$, a general Binomial random variable $B(n, p_n)$ converges in distribution to a Poisson random variable $Po(\lambda')$. Note that this proof is essentially just a restatement of

XV

the Poisson limit theorem of Poisson (1835).

$$\lim_{n \to \infty} \binom{n}{k} p_n^k (1 - p_n)^{n-k} = \lim_{n \to \infty} \frac{n \cdot (n-1) \cdot \ldots \cdot (n-k+1)}{k!} \left(\frac{\lambda'}{n}\right)^k \left(1 - \frac{\lambda'}{n}\right)^{n-k}$$

$$= \lim_{n \to \infty} \frac{n^k + O(n^{k-1})}{k!} \left(\frac{\lambda'}{n}\right)^k \left(1 - \frac{\lambda'}{n}\right)^{n-k}$$

$$= \frac{(\lambda')^k}{k!} \exp\left(-\lambda'\right)$$

Note that by definition τ is fixed and by assumption $a_i(y)$ is constant within $[t, t+\tau)$. Thus, $\lim_{dt \to 0} \frac{\tau}{dt} = \infty$, $\lim_{dt \to 0} a_i(y) \cdot dt = 0$ and $\frac{\tau}{dt} \cdot a_i(y) \cdot dt = \tau \cdot a_i(y)$. Using the convergence property mentioned above yields the result. $\qquad \square$

A.3.4 Polynomial basis

Theorem 2. $B_1(t) = 2t^3 - 3t^2 + 1$, $B_2(t) = t^3 - 2t^2 + t$, $B_3(t) = -2t^3 + 3t^2$, $B_4(t) = t^3 - t^2 \in \mathbb{R}_3(t)$ *form a polynomial basis of* $\mathbb{R}_3(t)$.

Proof. We need to show that the four polynomials are linearly independent. We do so by writing the polynomials in vector form, collect them in a matrix and show that this matrix has full rank.

$$\begin{pmatrix} 2 & 1 & -2 & 1 \\ -3 & -2 & 3 & -1 \\ 0 & 1 & 0 & 0 \\ 1 & 0 & 0 & 0 \end{pmatrix} \Leftrightarrow \begin{pmatrix} 0 & 0 & -2 & 1 \\ 0 & 0 & 1 & -1 \\ 0 & 1 & 0 & 0 \\ 1 & 0 & 0 & 0 \end{pmatrix} \Leftrightarrow \begin{pmatrix} 0 & 0 & 0 & -1 \\ 0 & 0 & 1 & -1 \\ 0 & 1 & 0 & 0 \\ 1 & 0 & 0 & 0 \end{pmatrix} \Leftrightarrow \begin{pmatrix} 0 & 0 & 0 & 1 \\ 0 & 0 & 1 & 0 \\ 0 & 1 & 0 & 0 \\ 1 & 0 & 0 & 0 \end{pmatrix}$$

Since $B_1(t), B_2(t), B_3(t), B_4(t)$ are four linearly independent polynomials of degree 3, they form a basis of $\mathbb{R}_3(t)$. $\qquad \square$

Schriftliche Versicherung

Ich versichere hiermit, dass ich die vorstehende Masterarbeit selbstständig verfasst und keine anderen als die angegebenen Quellen und Hilfsmittel benutzt habe, dass die vorgelegte Arbeit noch an keiner anderen Hochschule zur Prüfung vorgelegt wurde und dass sie weder ganz noch in Teilen bereits veröffentlicht wurde. Wörtliche Zitate und Stellen, die anderen Werken dem Sinn nach entnommen sind, habe ich in jedem einzelnen Fall kenntlich gemacht.

Ort, Datum   Unterschrift

Bonn, 26.07.2021